JIRRS
Journal International Review of Research Studies

Received: 13/06/2026 - **Accepted:** 07/11/2026
Vol: 1.11
DOI: 10.66104/bwxmzv70
Pages: 1-36

Beyond Chemical Purity: Optical Quality, Particle Morphology, Surface Modification, and Scale-Up of High-Whiteness Aluminum Hydroxide—A Critical Review

Antonio Clareti Pereira, Ph.D.
Department of Graduate Program in Materials Engineering
Federal University of Ouro Preto (UFOP)
Ouro Preto, Minas Gerais, Brazil
E-mail: claretipereira@gmail.com
ORCID: https://orcid.org/0000-0001-8115-4279

Abstract

High-whiteness aluminum hydroxide, principally gibbsite-based alumina trihydrate (ATH), is commonly specified using bulk impurity concentrations, although visual appearance also depends on chromophore speciation, particle architecture, agglomeration, sample preparation, and matrix interactions. This structured critical narrative review critically appraises 151 bibliographic records (147 from 2020–2026, two foundational studies from 2013 and 2018, and two colorimetry standards published or reaffirmed in 2019 and 2025). It distinguishes direct process and optical evidence from mechanistic, functional, and contextual evidence across Bayer-liquor purification, seeded precipitation, finishing, surface modification, qualification, and scale-up. A Whiteness-by-Design framework links impurity transport and aluminum recovery with particle properties, standardized CIELAB coordinates, spectral reflectance, qualified-product yield, and end-use evaluation. The evidence does not justify equating chemical purity, precipitation yield, high L^*, whiteness index, or matrix-level visual acceptance. Future industrial comparisons require paired mass balances and optical measurements under traceable specimen and application protocols.

Keywords: High-whiteness aluminum hydroxide; Alumina trihydrate; Gibbsite precipitation; Bayer liquor purification; Particle morphology; Functional mineral filler

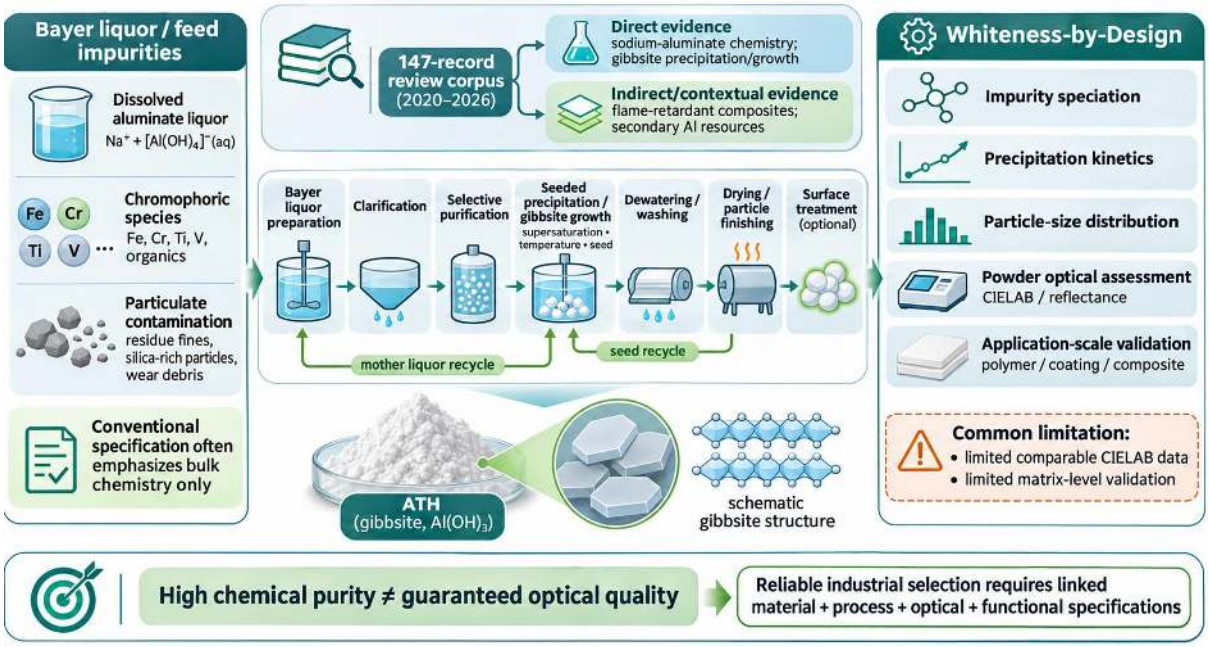
Highlights

- Bulk purity alone is insufficient to predict the optical appearance of ATH.
- Bayer-liquor chemistry and seeded growth jointly determine impurity retention.
- Finishing and surface treatment create benefits and risks for whiteness.
- Whiteness-by-Design requires standardized color and application testing.

JIRRS
Journal International Review of Research Studies

Received: 13/06/2026 - **Accepted:** 07/11/2026
Vol: 1.11
DOI: 10.66104/bwxmzv70
Pages: 1-36

Graphical Abstract



1. Introduction

Aluminum hydroxide, $Al(OH)_3$, is an essential intermediate of alumina production and a functional mineral filler. The gibbsite-rich grades marketed as alumina trihydrate (ATH) serve substantially different markets: specialty alumina precursors require limits on sodium and minor elements, whereas polymer and solid-surface applications additionally demand stable appearance, controllable viscosity, and appropriate particle architecture. Industrially meaningful whiteness is therefore a composite property, rather than a synonym for chemical purity. Recent publications examine gibbsite precipitation, liquor impurity removal, particle processing, and composite behavior separately, but do not necessarily report interchangeable product metrics (Bakhtom et al., 2023; Damjanović et al., 2025; Golubev et al., 2021; Wen et al., 2026).

This review asks how impurity identity and location, nucleation and growth history, and subsequent surface treatments interact to control the apparent color and application performance of ATH. The distinction between color and chemical concentration is central: a low total iron content does not exclude isolated dark particles, organic color bodies, or optical defects arising from poor dispersion. Figure 1 establishes the underlying process–structure–property hypothesis; Table 1 defines the corresponding evidence hierarchy. The discussion

JIRRS
Journal International Review of Research Studies

Received: 13/06/2026 - **Accepted:** 07/11/2026
Vol: 1.11
DOI: 10.66104/bwxmzv70
Pages: 1-36

uses the 151-record reviewed bibliography while retaining explicit uncertainty for peripheral studies and incomplete bibliographic metadata.

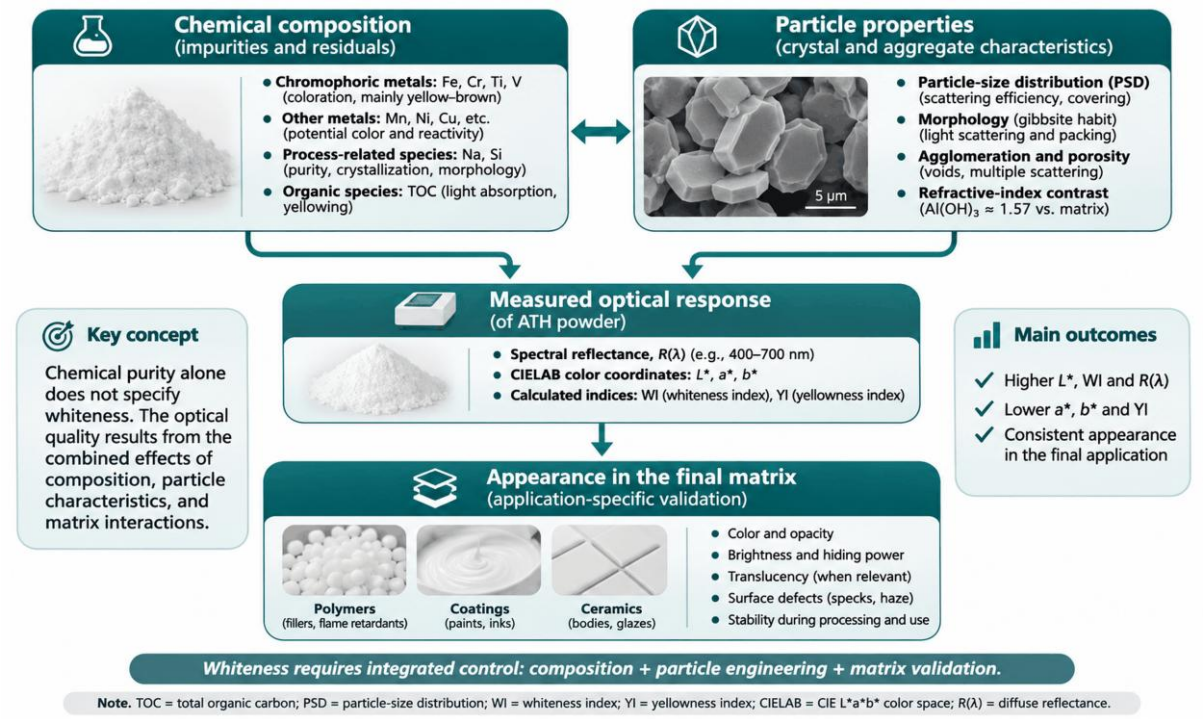


Figure 1. Coupled effects of chemical composition, particle characteristics, and matrix interactions on the optical quality of high-whiteness ATH.
Note. Conceptual schematic for this review. Illustration provenance and any AI-assisted creation disclosure must be checked against the author's original artwork records and the target journal policy before final submission.

The figure argues against reporting a single whiteness value without describing sample preparation and the receiving matrix. Instrumental reflectance on a compacted powder and perceived appearance in filled resin may respond differently to the same particle distribution.

2. Review Methodology and Critical Evidence Appraisal

2.1. Scope and search design

The initial supplied bibliography contains 147 references dated 2020–2026, assembled under 26 topic-specific Boolean search themes. Four necessary additions are two foundational publications (Sonthalia et al., 2013; Kim et al., 2018) and the ISO/CIE (2019) and ASTM International (2025) colorimetry standards, yielding 151 records, of which 148 (98.0%) are dated 2020–2026. This manuscript remains a structured critical narrative review,

JIRRS
Journal International Review of Research Studies
Received: 13/06/2026 - **Accepted:** 07/11/2026
Vol: 1.11
DOI: 10.66104/bwxmzv70
Pages: 1-36

not a systematic review. The supplied materials do not establish the exact final search date, a platform-specific export, the 26 verbatim Boolean expressions, a screening audit trail, or full-text verification of every record. These missing audit details must be documented from the actual research records before submission; they are not retrospectively reconstructed as if a systematic search had been conducted.

The novelty is the explicit integration of impurity chemistry, impurity location, particle architecture, standardized optical measurements, post-precipitation contamination controls, and matrix-specific qualification—not a claim to have first reviewed Bayer precipitation or ATH functional applications. Older foundational sources were included as targeted exceptions to the principal contemporary literature window because they directly address Bayer impurity effects and measured high-whiteness ATH production.

Search transparency: the precise final search date and verified platform list were not documented in the supplied manuscript. The 26 search themes should be archived as dated, platform-specific verbatim strings in supplementary material when the original search records are available. No PRISMA flow or systematic-review reproducibility is claimed.

2.2. Eligibility and weighting

Each record was appraised for relevance to the review question and for the type of inference justified by its available bibliographic information. Direct evidence includes work on gibbsite formation, sodium-aluminate purification, impurity incorporation, and ATH particle engineering. Mechanistic evidence includes physicochemical characterization with plausible transferability to Bayer products. Functional evidence concerns ATH-containing composites and coatings, and contextual evidence concerns upstream residues or environmental burdens. Titles and metadata alone do not establish the magnitude or statistical significance of experimental effects; quantitative claims are therefore avoided where primary results were not reviewed. Table 1 defines the four evidence classes used to separate direct evidence from contextual inference.

Table 1. Evidence classes and interpretive constraints.

Evidence class	Typical question	Permissible inference
Direct process	How does the Bayer circuit change gibbsite?	Route and variable identification

JIRRS
Journal International Review of Research Studies

Received: 13/06/2026 - **Accepted:** 07/11/2026
Vol: 1.11
DOI: 10.66104/bwxmzv70
Pages: 1-36

Evidence class	Typical question	Permissible inference
Mechanistic	Which uptake or growth pathway is possible?	Mechanistic hypothesis, not guaranteed whiteness
Functional	How does ATH behave in a matrix?	Formulation-specific behavior
Contextual	What are sustainability or recycling issues?	Boundary conditions, not product optical proof

Note. Classification is a critical-appraisal framework constructed for this review, not an experimental ranking.

An essential quality distinction is between analytical completeness and evidential relevance. A study with a resolvable DOI may still lack standardized reflectance measurements, a reliable baseline, or representative industrial scale. We retained such studies for contextual comparison but did not cite them as proof of high whiteness.

Critical appraisal was organized around four independent outcome classes: (i) dissolved-impurity removal and aluminum recovery, (ii) gibbsite phase, morphology, and particle-size distribution, (iii) instrumental optical attributes using a fully stated measurement protocol, and (iv) end-use performance in a controlled reference formulation. Evidence measuring only one class is not treated as proof of improvement in the others. Because an exhaustive full-text verification and reproducible search-export record are not available for all supplied references, the review remains a structured critical synthesis rather than a systematic or meta-analytic review.

3. Terminology, Grades, and Application Specifications

The terms aluminum hydroxide, alumina trihydrate, ATH, and gibbsite are not fully interchangeable. ATH designates $Al(OH)_3$ chemistry and is commonly associated with gibbsite; bayerite and nordstrandite are alternative trihydroxide polymorphs, whereas boehmite and pseudoboehmite are oxyhydroxide-based materials. Phase discrimination matters because thermal response, specific surface, and processing history vary with phase identity. Studies concerned with boehmite-derived specialty alumina provide precursor context rather than direct whiteness evidence (Gasparini et al., 2022; Wen, Liu, Qi, Liu, et al., 2026; Yang et al., 2024).

A useful specification separates chemical, morphological, optical, and functional dimensions. The optical dimension must report at least instrumental color coordinates and measurement geometry; the particle dimension should include D_{10}, D_{50}, D_{90}, morphology,

JIRRS
Journal International Review of Research Studies
Received: 13/06/2026 - **Accepted:** 07/11/2026
Vol: 1.11
DOI: 10.66104/bwxmzv70
Pages: 1-36

and agglomeration; and the chemical dimension should distinguish soluble sodium from residual total sodium and particulate from dissolved contaminants. End-use acceptance should be established in the intended formulation. Table 2 summarizes the corresponding minimum specifications.

Table 2. Minimum multiaxial specification for high-whiteness ATH.

Attribute	Recommended reporting	Why required
Chemical	$Al(OH)_3$, Fe, Cr, Ti, Si, total/soluble Na, TOC	Chromophores and soluble contaminants
Particles	$D_{10}/D_{50}/D_{90}$, SEM, agglomerates, BET	Scattering and processing response
Optical	L^*, a^*, b^* (ISO/CIE 11664-4); WI/YI (ASTM E313, only where applicable); ΔE^*_{ab}; reflectance spectrum; specimen protocol	Reproducible color comparison
Handling	Moisture, oil absorption, packing, foreign specks	Lot stability and visual defects
End-use	Color, viscosity, aging and performance in matrix	Acceptance cannot rely on powder only

Note. Proposed reporting framework; no universal industrial threshold is asserted.

A universal threshold for "high whiteness" cannot be inferred from the supplied studies. Market-facing ATH grades should therefore be benchmarked against application-specific reference materials rather than a single instrument reading.

This distinction also applies to metrics: CIELAB L^* is a lightness coordinate, whereas indices of whiteness and yellowness depend on the instrument method and calculation convention. For a reproducible comparison, measurements require the same illuminant, standard observer, geometry, specimen thickness/packing, background, and moisture conditioning. A shift in the b^* coordinate may signal unacceptable yellowing even when L^* is high; conversely, an improved reflectance reading for loose powder does not establish acceptable translucency in a resin composite.

Formal colorimetric reporting should follow ISO/CIE 11664-4:2019 (confirmed in 2024) for CIELAB coordinates and ASTM E313-20(2025) for the applicable whiteness and yellowness index calculations. L^* represents lightness, not a universal whiteness index; WI is not L^*, and YI is not b^*. Report the exact WI/YI calculation, reference white, observer, illuminant and specimen class, and do not compare ASTM indices outside the standard's

JIRRS
Journal International Review of Research Studies
Received: 13/06/2026 - **Accepted:** 07/11/2026
Vol: 1.11
DOI: 10.66104/bwxmzv70
Pages: 1-36

material-appearance and applicability constraints (ISO/CIE, 2019; ASTM International, 2025).

A mandatory powder-color protocol should record specimen preparation (loose/packed/pressed), any compaction pressure, bed thickness, leveling, backing, conditioning humidity and moisture, aperture, instrument geometry, illuminant, observer, calibration, number of replicate positions, and within-lot variability. Record spectral reflectance R(λ), ideally over 400–700 nm or the instrument's documented visible range, when mechanisms of blue-region absorption or scattering are investigated.

4. Fundamentals of Whiteness and Impurity Retention

4.1. Optical mechanisms

Lightness (L^*) expresses a perceptual coordinate; the a^* and b^* coordinates encode red–green and yellow–blue directions. A whiteness index, yellowness index, brightness measurement, and spectral reflectance are different reported quantities. Interpreting them requires the illuminant, observer, instrument geometry, sample packing, and reference standard. The same particle chemistry can therefore generate non-equivalent numerical appearance assessments. Particle shape and porosity modify multiple scattering, while adsorbed color bodies introduce wavelength-dependent absorption.

For a sufficiently optically thick, diffusely reflecting specimen under the assumptions of the two-flux Kubelka–Munk approximation, $F(R_\infty) = (1 - R_\infty)^2/(2R_\infty) = K/S$, where K and S are effective absorption and scattering coefficients. This conceptual relation is not universally exact for loose, nonuniform ATH powder beds: K/S may change because of chromophore absorption, particle-scale scattering, or both. Thus identical elemental assays need not produce identical optical response.

For lot-to-reference comparison, report $\Delta L^* = L^*_{lot} - L^*_{reference}$, $\Delta b^* = b^*_{lot} - b^*_{reference}$, and $\Delta E^*_{ab} = [(\Delta L^*)^2 + (\Delta a^*)^2 + (\Delta b^*)^2]^{(1/2)}$. If CIEDE2000 is used instead, identify the alternative metric and calculation, rather than labeling it ΔE^*_{ab}.

JIRRS
Journal International Review of Research Studies

Received: 13/06/2026 - **Accepted:** 07/11/2026
Vol: 1.11
DOI: 10.66104/bwxmzv70
Pages: 1-36

4.2. Mechanisms of impurity deportment

Figure 2 distinguishes impurity pathways that total elemental analysis alone cannot resolve. Metal ions may remain dissolved, associate with surfaces, become occluded in a growing aggregate, or be incorporated in a crystal lattice; mechanically introduced foreign particles create an additional defect class. Recent structural investigations of metal incorporation and gibbsite perturbation provide a mechanistic basis for these distinctions (Zhang et al., 2023; Zhao et al., 2024). However, observing a crystal-level interaction does not by itself establish a measured change in commercial whiteness.

Impurity deportment can be expressed as $D_{M,k} = m_k \cdot C_{M,k}/[m_F \cdot C_{M,F}]$ for impurity M in product/host class k relative to a defined feed F, provided the classes and dry-mass boundaries are consistent. The sum of fractions must include solution, solids, deposits, residue and losses to close the impurity balance; a crystal-incorporated Fe or Cr species must not be conflated with particulate Fe-rich specks. Zhao et al. (2024) furnish especially relevant mechanistic evidence for trace Fe/Cr incorporation, but not a direct measurement of commercial whiteness.

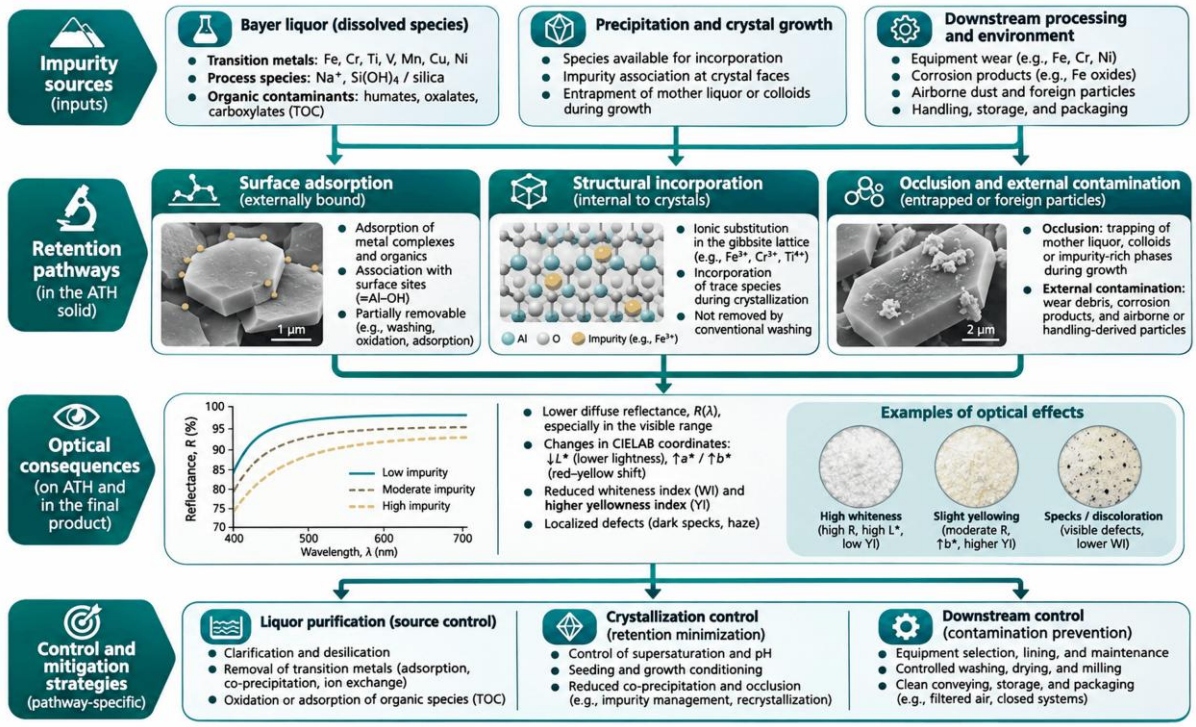


Figure 2. Impurity sources, retention pathways, optical consequences, and control strategies in high-whiteness ATH production.

JIRRS
Journal International Review of Research Studies
Received: 13/06/2026 - **Accepted:** 07/11/2026
Vol: 1.11
DOI: 10.66104/bwxmzv70
Pages: 1-36

Note. Conceptual schematic for this review. Illustration provenance and any AI-assisted creation disclosure must be checked against the author's original artwork records and the target journal policy before final submission.

The route selected to remove a contaminant must match its chemical state and location. Dissolved iron may require targeted liquor treatment, whereas an isolated dark speck from equipment wear is more appropriately addressed by material-of-construction control and particulate removal. A single bulk impurity limit cannot identify both failure modes.

4.3. Organic matter and colloidal contaminants

Organics accumulate from bauxite-derived species and recycled Bayer liquor, with effects that depend on their molecular forms, interactions with growing solids, and processing conditions. The corpus includes work on oxidation, adsorption, flotation, and coupled organic treatment (Fu, Liu, Qi, Shen, Peng, Li, et al., 2024a; Fu, Liu, Qi, Shen, Peng, Li, et al., 2024b; Ran et al., 2022; Wu et al., 2022; Zhang et al., 2020). Their practical value depends not only on total organic carbon reduction but also on removal of chromophoric compounds, prevention of adverse precipitation behavior, and control of treatment-derived residues. Table 3 links each impurity class to a diagnostic and control strategy.

Total organic carbon (TOC) quantifies organic carbon, not chromophore strength. Studies asserting a color benefit should pair TOC with UV–Vis absorbance (and molecular speciation when feasible), while documenting final ATH reflectance and color under the same measurement protocol. Count isolated black specks by area or mass using image analysis, and use SEM–EDS or appropriately validated magnetic separation tests to investigate source and composition.

Table 3. Impurity classes, potential retention mechanisms, and targeted control.

Contaminant	Pathway	Diagnostic/corrective logic
Fe/Cr and transition metals	Speciation, adsorption, substitution, particles	ICP plus microscopy/EDS; selective removal
Organic color bodies	Solution persistence, surface adsorption	TOC plus UV–Vis; liquor oxidation/adsorption
Silica and sodium	Desilication species, soluble liquor carryover	Phase/XRF and soluble sodium; wash/clarify
Foreign specks	Wear, dust, filtration failure	Particle counts, magnetic separation, SEM–EDS

JIRRS
Journal International Review of Research Studies
Received: 13/06/2026 - **Accepted:** 07/11/2026
Vol: 1.11
DOI: 10.66104/bwxmzv70
Pages: 1-36

Note. Qualitative mechanism map; specific limits require experimental validation.

The central interpretive result is that impurity removal efficiency and whiteness improvement are related only through measured optical outcomes. An apparently successful purification campaign may fail if chromophoric organics, solids carryover, and post-precipitation contamination are not distinguished.

5. Feedstocks and Industrial Impurity Pathways

Feedstock variability arises from bauxite mineralogy, reactive silica, iron-bearing phases, carbonaceous material, and trace elements. Liquor quality reflects digestion chemistry and recycled stream history, not simply the head assay of bauxite. Research on silica behavior, potassium during digestion, and sodium-aluminate solution structure provides relevant process context (Abdulvaliyev et al., 2025; Chen et al., 2024; Gao et al., 2026; Gasparini et al., 2022). These studies establish candidate variables for monitoring rather than a transferable commercial whiteness guarantee.

Non-Bayer sources, including secondary dross and anodizing sludge, are frequently described as circular pathways to recover aluminum compounds (Acosta et al., 2025; Chen et al., 2024; Dyussenova et al., 2026; Gao et al., 2026; Pereira, 2026a; Pereira, 2026e; Tang et al., 2022; Tang et al., 2024; Wu et al., 2025; Zhang et al., 2023). However, extraction yield is an insufficient success criterion for optical-grade ATH. Each route must demonstrate reagent carryover, chromophoric trace-element removal, stable crystal phase, and post-treatment color under the same conditions used for primary products.

A critical industrial blind spot concerns equipment-derived contamination after liquor purification. Filter media, steel surfaces, grinding contacts, dryer internals, conveyors, and packaging can create low-frequency high-contrast specks that average bulk assays overlook. Particle counting and source attribution must accompany conventional chemical characterization.

6. Purification of Sodium Aluminate Solutions

6.1. Inorganic purification

Clarification and polishing filtration target suspended solids, whereas dissolved species require chemically selective operations. In real sodium-aluminate liquors,

JIRRS
Journal International Review of Research Studies
Received: 13/06/2026 - **Accepted:** 07/11/2026
Vol: 1.11
DOI: 10.66104/bwxmzv70
Pages: 1-36

Damjanović et al. (2025) examined Fe, Zn, and Cu removal using finely precipitated hydroxide: greater specific surface area promoted metal uptake but also accelerated aluminum hydroxide crystallization and the associated loss of dissolved alumina. Their results therefore demonstrate a measurable purity–yield trade-off, not a direct gain in optical whiteness. In their reported conditions, Cu and Fe were removed more rapidly than Zn; the material balance and impurity localization should be reassessed before transferring the method to an optical-grade precipitation circuit. Dai et al. (2025) investigated fluoride removal by double-salt crystallization, while Liu et al. (2024) addressed potassium separation. These routes affect different impurity inventories and should not be ranked on removal percentage alone; sodium balance, solid residues, final particle color, and recycle stability are essential comparable endpoints.

For each purification route, a common reporting basis should include $R_i = 100[m_{i,F} - m_{i,P}]/m_{i,F}$ for a clearly specified impurity input/output boundary and $R_{Al} = 100m_{Al,desired\ circuit}/m_{Al,F}$, as well as reagent consumption, residue and purge loads, recycles, aluminum losses, and the measured optical differences ΔL^*, Δb^* and ΔE^*_{ab}. Dissolved-species treatment and solids clarification must not be pooled as equivalent mechanisms.

6.2. Organic control and process trade-offs

Advanced oxidation and precipitation-assisted methods can alter soluble organics but must be compared on actual liquor rather than unrelated model wastewaters. The bibliography includes an experimental thesis on ozonation and a thesis on Bayer liquor purification (Moreno, 2020; Soplin Pastor, 2021). Their evidential status must remain differentiated from independently replicated industrial investigations. A correct techno-economic comparison includes caustic consumption, aluminum loss, recycle compatibility, residue handling, and color stability.

The conceptual flowsheet in Figure 3 places final particle quality downstream of, but not equivalent to, liquor treatment. Purification should be intensified only as far as demonstrable optical and functional improvement justifies reagent and waste burdens.

JIRRS
Journal International Review of Research Studies
Received: 13/06/2026 - **Accepted:** 07/11/2026
Vol: 1.11
DOI: 10.66104/bwxmzv70
Pages: 1-36

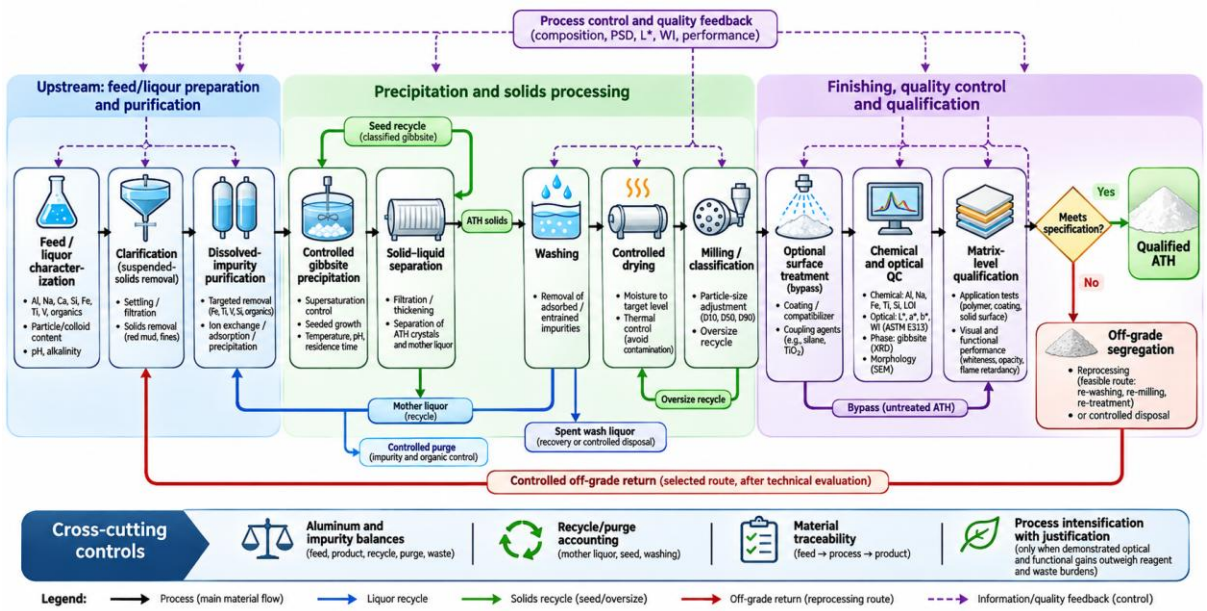


Figure 3. Integrated conceptual ATH production architecture, including liquor purification, controlled precipitation, separation, recycle streams, finishing, and quality control.
Note. Original document-native qualitative process schematic developed for this review; no universal numerical setpoints or grade limits are implied.

The figure separates upstream removal of dissolved species from downstream removal of soluble liquor and accidental particulate contaminants. It also highlights that the final instrument measurement is a process feedback variable, not a substitute for upstream mass balances.

7. Precipitation, Nucleation, and Crystal-Growth Engineering

Supersaturation drives gibbsite nucleation and growth, while seed area, temperature, agitation, residence-time distribution, liquor composition, and recycled fines shape the evolving particle population. Recent studies address growth inhibition by anions, intermediary aluminate species, and precipitation in laboratory and reduced-scale tanks (Bakhtom et al., 2023; Bakhtom et al., 2025; Chen et al., 2025; Graham, Ghandi, et al., 2026; Graham et al., 2022; Graham, Kennedy, et al., 2026; Graham et al., 2023; Graham, Prange, et al., 2026; Shoppert et al., 2023; Wang et al., 2024; Wang et al., 2025). The studies are not directly interchangeable because seed condition and hydrodynamic scale often differ.

The mechanistic foundations described by Sonthalia et al. (2013) link Bayer-liquor impurities to hydrate growth and agglomeration. Particle-population reporting should distinguish primary crystal shape, agglomeration and fines; include D_{10}, D_{50}, D_{90} and span =

JIRRS
Journal International Review of Research Studies
Received: 13/06/2026 - **Accepted:** 07/11/2026
Vol: 1.11
DOI: 10.66104/bwxmzv70
Pages: 1-36

$(D_{90} - D_{10})/D_{50}$, and, where practical, aspect ratio, platelet thickness, roundness and surface roughness. These variables can influence scattering even at the same D_{50}.

Kim et al. (2018) provide direct high-whiteness product evidence: caustic roasting and water leaching of low-grade bauxite, followed by precipitation, yielded ATH of D_{50} 1.9–2.8 µm and reported whiteness index 96.8–97.5 under the authors' conditions. Their index must not be numerically equated with CIELAB L^* or transferred between instruments without checking the primary study's measurement and specimen methods.

Seeded decomposition and carbonation provide different supersaturation pathways and should not be assumed to produce interchangeable ATH. Bakhtom et al. (2023) tested a 1/100-scale tank with industrial Bayer liquor. The supplied manuscript reports a 46–53% increase in precipitation extent under selected response-surface conditions; the magnitude and comparison basis require confirmation in the primary publication (50 °C, 230 rpm, and seed concentration of 327 g/L). This is evidence for improved precipitation extent within that apparatus, not evidence of greater whiteness, reduced black-speck counts, or industrially transferable hydrodynamics. Its significance for optical-grade ATH depends on accompanying particle-size distributions, impurity partitioning, filtration performance, and standardized colorimetry. Laboratory observations of anion-specific changes in gibbsite crystallization (Chen et al., 2025) provide a complementary mechanistic warning: crystal-growth responses are impurity-specific and must be distinguished from the operating chemistry of a hot caustic Bayer liquor.

Population balance models can link size distributions with nucleation, breakage, agglomeration, and growth. However, fitting precipitation yield alone is not enough: the same mass of recovered $Al(OH)_3$ can be distributed among a coarse product, excessive fines, or fragile agglomerates. An optical-grade process must follow particle populations and impurity uptake together. Table 4 compares the process variables affecting crystal growth and potential quality trade-offs.

Table 4. Precipitation variables and interpretation of optical-grade product quality.

Variable	Primary effect	Potential trade-off
Supersaturation	Nucleation versus growth balance	Fine-particle generation
Seed activity and loading	Growth sites and PSD	Occlusion and carryover

JIRRS
Journal International Review of Research Studies
Received: 13/06/2026 - **Accepted:** 07/11/2026
Vol: 1.11
DOI: 10.66104/bwxmzv70
Pages: 1-36

Variable	Primary effect	Potential trade-off
Temperature and mixing	Kinetics and heterogeneity	Local growth instability
Carbonation regime	Driving force and pH trajectory	Sodium/carbonate balance
Residence-time distribution	Product uniformity	Batch-to-batch variability

Note. Effects are mechanistic hypotheses requiring scale-specific confirmation; no universal operating setpoints are prescribed.

The evidence supports an integrated interpretation of crystal engineering: improving precipitation efficiency is useful, but whiteness remains an additional response variable requiring explicit measurement. Better yield and visually preferable crystal architecture are not necessarily equivalent.

8. Filtration, Washing, Drying, Milling, and Classification

Separation efficiency, washing, and finishing determine whether upstream purity gains survive. Filtration and washing reduce soluble sodium and mother liquor; drying changes residual moisture and agglomeration; milling and classification reshape the particle-size distribution and can introduce wear products. Bibliographic records addressing drying, sodium elimination, active seeds, micronization, and particle form provide targeted context (Dong et al., 2020; Gorla et al., 2022; Pereira, 2026c; Silva et al., 2020; Wen, Liu, Qi, Liu, et al., 2026; Yang et al., 2025; Zheng et al., 2024).

A washing study should report stage-wise wash-water use, total and soluble Na, conductivity, mother-liquor displacement, dissolved Al losses, and any changes in powder color. Drying quality control should track residence time, thermal history, final moisture, phase composition, agglomeration, $L^*a^*b^*$ coordinates, and speck counts. Milling trials should identify grinding media, liners, contact materials, ferrous wear, Fe assays before/after milling, fines generation, and any magnetic traps or clean-air packaging barriers.

Drying is particularly critical because aggressive thermal exposure can alter hydroxide phase and surface characteristics. Temperature and residence-time limits should be established from moisture and phase-composition measurements, not from energy efficiency alone. A dryer that meets moisture targets but increases dark specks or shifts color is not qualified for optical-grade production.

A robust classification strategy controls D_{10}, D_{50}, D_{90}, oversize, and high-energy tail fines. Excessive comminution increases specific surface, potentially worsening slurry

JIRRS
Journal International Review of Research Studies
Received: 13/06/2026 - **Accepted:** 07/11/2026
Vol: 1.11
DOI: 10.66104/bwxmzv70
Pages: 1-36

rheology and resin demand. Magnetic separation, clean-air handling, and clean packaging remain important even after achieving the target particle-size distribution.

9. Surface Modification and Formulation Compatibility

Hydrophilic ATH requires deliberate compatibility management in hydrophobic polymer matrices. Silanes, fatty-acid derivatives, polymeric coatings, and reactive or inorganic shells may improve dispersion or interface adhesion while modifying processing viscosity. The bibliography contains multiple studies of coated or modified ATH in EVA, polyolefin, epoxy, polyurethane, and other polymers (Cheng et al., 2025; Doanh et al., 2025; Dou et al., 2025; Dukarski et al., 2021; Ferrante et al., 2026; Scionti et al., 2023; Shaker et al., 2023; Sung et al., 2023; Sung et al., 2026; Sung et al., 2024; Uddin et al., 2022; Wang et al., 2025; Xing, Li, Liu, Qi, et al., 2025; Xing, Li, Liu, Yang, et al., 2025; Zheng et al., 2025). Most primarily measure fire or mechanical outcomes and should not be treated as direct evidence of high whiteness.

Surface modification may also change color through reagent oxidation, incomplete coating, or a shift in refractive-index contrast. Consequently, reporting only a limiting oxygen index or tensile strength leaves a gap in quality assessment. Coating assessment should combine FTIR or XPS, thermal and surface-energy measurements, color before and after treatment, and aging under application conditions.

For coated ATH, report modifier identity and dose, coating coverage, before/after color, FTIR/XPS or equivalent surface evidence, dispersion and viscosity in the intended matrix, and color after storage and relevant UV/thermal aging. Improved flame retardancy or mechanical strength alone cannot establish improvement in optical appearance.

10. Characterization and Standardized Optical Quality

Quality assurance must be multi-instrumental. XRF, ICP-OES/MS, ion chromatography, and carbon analysis reveal bulk chemistry; XRD, FTIR, Raman, and TGA provide phase and thermal evidence; SEM–EDS and particle sizing resolve morphology and foreign particles. Colorimetry requires L^*, a^*, b^*, documented illuminant and observer, geometry, aperture, sample preparation, and independent replicate readings. Differences

JIRRS
Journal International Review of Research Studies
Received: 13/06/2026 - **Accepted:** 07/11/2026
Vol: 1.11
DOI: 10.66104/bwxmzv70
Pages: 1-36

between powder beds, pellets, coatings, and composites require explicit testing rather than assumed equivalence.

Figure 4 formalizes a linked measurement chain. The critical audit question is not whether a study reports many parameters, but whether it can connect a specific process intervention with an optical response after controlling other confounders. Formulation tests must include reference material, blank matrix, storage stability, and uncertainty where possible.

Minimum acceptance protocol: qualify powder against a reference lot with replicate optical readings and test a controlled resin or coating formulation with documented polymer identity, filler loading, mixing and curing conditions, specimen thickness, backing, surface preparation/polishing, color difference, translucency (where relevant), visible defects, aging and viscosity. Whiteness-by-Design (WbD) is presented here as an application of quality-by-design (QbD) principles to a linked process–structure–optical–application control chain.

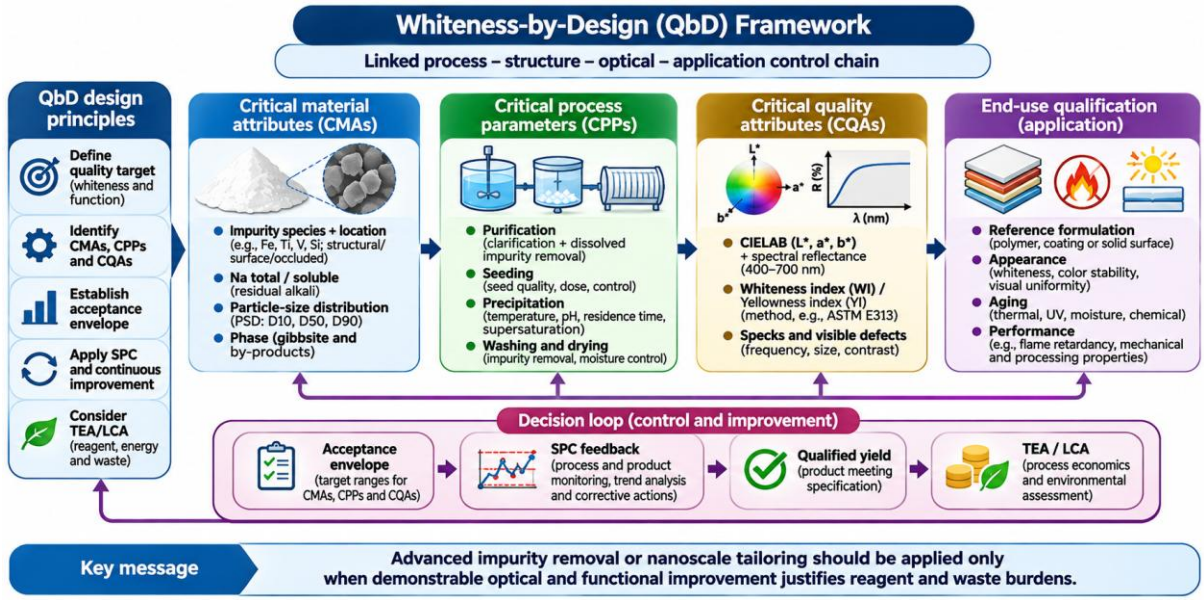


Figure 4. Whiteness-by-Design framework linking critical material attributes, process parameters, verified optical outcomes and application-specific qualification.
Note. Original document-native qualitative WbD/QbD framework for this review; acceptance limits must be established and verified for a specified product grade and end-use.

The framework identifies a common evidentiary disconnect: sophisticated nanoscale or mechanistic experiments can reveal scientifically important interactions but remain insufficient to predict industrial surface appearance. Quantitative cross-scale validation is a

JIRRS
Journal International Review of Research Studies
Received: 13/06/2026 - **Accepted:** 07/11/2026
Vol: 1.11
DOI: 10.66104/bwxmzv70
Pages: 1-36

major research priority. Table 5 identifies measurement methods and reporting controls needed to interpret optical quality.

Table 5. Proposed analytical panel and minimum reporting requirements.

Method	Reported outcome	Critical qualification
ICP/XRF/TOC	Trace metals, major oxides, organic load	Detection limits and sampling location
XRD/SEM–EDS	Phase, particle morphology, speck identity	Representative images and phase fractions
Laser diffraction	D_{10}, D_{50}, D_{90} and span	Dispersion protocol and repeatability
Colorimeter/spectrometer	L^*, a^*, b^* (ISO/CIE 11664-4); WI/YI (ASTM E313, only where applicable); ΔE^*_{ab}; reflectance spectrum; specimen protocol	Illuminant, observer, geometry, reference
End-use trial	Viscosity, appearance, thermal/mechanical performance	Control formulation and aging

Note. Recommended study reporting variables; match test standards to the target market.

11. Application-Specific Structure–Property–Performance

11.1. Solid-surface and specialty applications

Solid-surface products are particularly sensitive to yellow hue, inconsistent translucency, agglomerates, oil absorption, and visible foreign inclusions. Particle packing and matrix index contrast can dominate appearance even when chemical purity is comparable. Conversely, a precursor for specialty alumina requires special attention to sodium and phase transformation during calcination. Research on hydroxide-derived alumina and ceramic precursors is relevant only to that precursor-specific use case (Chen et al., 2025; Wen, Liu, Qi, Liu, et al., 2026; Wen et al., 2025; Zheng et al., 2025).

11.2. Flame-retardant polymers and coatings

ATH undergoes endothermic decomposition with water liberation, contributing to cooling and dilution in suitable fire-retardant formulations. However, higher filler fractions may reduce processability or mechanical performance. Reported advances in fire-retardant systems illustrate the need to balance interface treatment, filler size, loading, mechanical integrity, and combustion metrics (Cheng et al., 2025; Dou et al., 2025; Hu et al., 2023; Ji et al., 2024; Liu et al., 2022; Scionti et al., 2023; Shaker et al., 2023; Sung et al., 2023; Sung et

JIRRS
Journal International Review of Research Studies
Received: 13/06/2026 - **Accepted:** 07/11/2026
Vol: 1.11
DOI: 10.66104/bwxmzv70
Pages: 1-36

al., 2024; Xing, Li, Liu, Qi, et al., 2025; Xing, Li, Liu, Yang, et al., 2025; Zheng et al., 2025; Zhu et al., 2024). Different polymer systems cannot be ranked by ATH whiteness unless standardized color data are reported.

Flammability outcomes, including limiting oxygen index, cone calorimetry, smoke evolution, and classification ratings, are distinct from optical quality metrics. For visible products, a fire-performance optimum may be commercially unsuitable if it produces unacceptable color drift, specking, or surface roughness. Table 6 summarizes application-specific acceptance metrics and unresolved evidence gaps.

Table 6. Application-specific success criteria and principal blind spots.

Application	Primary acceptance metrics	Evidence gap
Artificial stone / solid surfaces	CIELAB, translucency, viscosity, specks	Powder-to-resin color transfer
Cables and elastomers	Fire behavior, smoke, rheology, elongation	Aging and electrical property balance
Coatings and adhesives	Color, dispersion, coating integrity	Substrate and weathering dependence
Specialty alumina	Na, phase purity, morphology	Precursor-to-calcine property transfer

Note. No universal acceptance thresholds are assigned without customer specifications.

12. Industrial Scale-Up, Economics, and Sustainability

Industrial production must maintain a stable material balance between alumina recovery, sodium recycle, impurity purge, water use, and residue production. Higher-purity streams add costs not only in purification reagents but also in product losses, filtration demand, drying energy, classification recycle, and rejection of off-color lots. Dynamic simulation and scale-up work is relevant to reactor representativeness, residence-time distribution, and process control (Bakhtom et al., 2023; Golubev et al., 2021; Litvinova et al., 2026; Pereira, 2026b; Pereira, 2026c; Pereira, 2026d; Zhou et al., 2023).

Aluminum and impurity closure should be stated for every process and recycle boundary: $m_{Al,in} = m_{Al,qualified\ ATH} + m_{Al,off\text{-}grade} + m_{Al,residues} + m_{Al,purge} + \Delta M_{Al,inventory}$, with corresponding component-wise equations for Fe, Cr, Ti, Ni/Mn where relevant, Si, Na and organic carbon. Recycle and purge inventories must be quantified before claiming steady-state impurity control.

JIRRS
Journal International Review of Research Studies
Received: 13/06/2026 - **Accepted:** 07/11/2026
Vol: 1.11
DOI: 10.66104/bwxmzv70
Pages: 1-36

For each application-specific acceptance envelope, qualified yield $Y_q = m_{qualified\ ATH}/m_{total\ ATH}$. Economic, energy, fresh-water and waste indicators should be normalized respectively as total cost, total energy, fresh-water mass and waste mass divided by $m_{qualified\ ATH}$; the rejected, reworked and recycled streams remain in the system boundary. TEA should state currency, cost year, annual production, caustic and reagent consumption, electricity and thermal energy, alumina loss, filtration, drying, classification, wastewater/residue treatment and off-grade handling. LCA must document boundaries, allocation and uncertainty and cannot assume secondary feedstocks are inherently superior.

Life-cycle comparisons need common functional units and boundaries. Circular processing that consumes additional caustic, produces more waste, or substantially increases electricity demand may not outperform a primary route for a given optical-grade product. Contextual sustainability studies can identify these questions but cannot establish an ATH-specific environmental advantage without a consistent purity and performance benchmark (Dyussenova et al., 2026; Ma et al., 2022; Pereira, 2026a; Pereira, 2026d; Pereira, 2026e; Tang et al., 2022; Tang et al., 2024; Wu et al., 2025; Zhou et al., 2023).

A Whiteness-by-Design strategy treats feedstock attributes, liquor composition, seed distribution, finishing intensity, and end-use performance as linked critical quality attributes. The appropriate industrial comparison is not minimum process cost per tonne of any hydroxide, but cost per tonne of qualified, application-appropriate high-whiteness ATH. Table 7 organizes the principal industrial scale-up risks and monitoring responses.

Table 7. Scale-up risk register for application-qualified ATH.

Risk	Early warning signal	Mitigation/evidence
Recycle impurity buildup	Rising organics/metal speciation	Purges and liquor balances
PSD drift	$D_{10}/D_{50}/D_{90}$ changes	Population-balance monitoring
Optical contamination	b^* drift or speck count	Source mapping and clean handling
Off-grade production	Composite color failure	End-use qualification and SPC
Environmental burdens	Water, energy, residue per qualified mass	Consistent LCA and TEA boundary

JIRRS
Journal International Review of Research Studies
Received: 13/06/2026 - **Accepted:** 07/11/2026
Vol: 1.11
DOI: 10.66104/bwxmzv70
Pages: 1-36

Note. Qualitative process-engineering synthesis. SPC = statistical process control; LCA = life-cycle assessment; TEA = techno-economic assessment.

12.1. Research Gaps and Validation Roadmap

The main unresolved question is the causal mapping from impurity speciation to measured optical quality under industrial precipitation and finishing conditions. Future studies should publish complete color protocols, impurity phase/speciation balances, matched reference ATH materials, reproducible particle-size distributions, and appearance changes after formulation and aging. Experiments that vary purification severity while holding precipitation and particle finishing constant would directly test whether impurity removal produces a meaningful whiteness benefit.

A second research priority is linking population-balance crystallization models with chromophore uptake and particle optics. A third is distinguishing laboratory reports of precursor recovery from repeatable industrial production of application-qualified ATH, using transparent yields, impurity purges, energy, water, and rejects on a common functional basis.

A practical validation program should therefore use paired lots of ATH processed under controlled purification severity while holding the seed population and finishing sequence constant. The minimum response set would include liquor impurity speciation, precipitation yield, $D_{10}/D_{50}/D_{90}$, total and soluble sodium, Fe-bearing foreign-particle counts, spectral reflectance, CIELAB coordinates, repeatability, and the appearance of a standard resin plaque before and after accelerated aging. Reported quality improvements would then be traceable to a process intervention rather than confounded by simultaneous changes in particle size or surface treatment.

A practical evidence-to-qualification hierarchy is: (1) close material and impurity balances; (2) measure powder phase, PSD, morphology and optical response under controlled preparation; (3) demonstrate lot-to-lot color and speck stability; (4) compare reference formulations and aging; and (5) confirm process operability, statistical process control and economic/environmental metrics per tonne of application-qualified ATH. Pilot data, plant data and simulations should remain explicitly differentiated.

JIRRS
Journal International Review of Research Studies

Received: 13/06/2026 - **Accepted:** 07/11/2026
Vol: 1.11
DOI: 10.66104/bwxmzv70
Pages: 1-36

13. Conclusions

High-whiteness aluminum hydroxide should be engineered as an application-specific optical and functional particulate system rather than qualified solely by bulk chemical purity. Solution purification is necessary for many impurity pathways but insufficient where particulate contamination, occlusion, morphology, agglomeration, drying, or surface treatment alter final appearance. Seeded precipitation and particle finishing require joint optimization because increasing hydroxide yield does not automatically produce the most suitable optical particle architecture. Instrumental color on the powder must be connected to appearance, stability, and rheology in the intended matrix. The Whiteness-by-Design framework offers a practical basis for linking feedstock selection, purification, particle engineering, standardized color measurement, and industrial performance. Its predictive value remains to be validated through controlled cross-scale experiments and explicit quality, economic, and environmental balances.

Declarations

Funding

Funding

This review received no specific external funding.

Conflict of Interest

The author declares no conflict of interest.

Data Availability

No new experimental datasets were generated. All quantitative values discussed in the review are traceable to the cited literature.

Author Contributions

The author performed conceptualization, critical analysis, literature synthesis, visualization, and manuscript preparation.

References

Abdulvaliyev, R., Gladyshev, S., Akhmadiyeva, N., Ruzakhunova, G., & Tugambay, S. (2025). Influence of silica on the crystallization of sodium hydroaluminate. Complex Use of Mineral Resources, 333(2), 71–79. https://doi.org/10.31643/2025/6445.19

JIRRS
Journal International Review of Research Studies

Received: 13/06/2026 - **Accepted:** 07/11/2026
Vol: 1.11
DOI: 10.66104/bwxmzv70
Pages: 1-36

Acosta, F., Feijoo, C., Sangurima-Cedillo, A. S., Guevara, A., & Aragón-Tobar, C. F. (2025). Upcycling anodic sludge from aluminum anodizing: Leaching efficiency and thermal conversion into refractory materials. Sustainability, 17(18), 8491. https://doi.org/10.3390/su17188491

Ait El Mahjoub, A., Najid, N., Falil, F. Z., Rashwan, H. A., Stiriba, Y., Audonnet, F., Vial, C., Necibi, M. C., & Gourich, B. (2025). Optimizing and predicting electrocoagulation performance for simultaneous removal of fluoride, silica, and hardness from real brackish groundwater: Integrating response surface methodology with interpretable machine learning. Journal of Environmental Chemical Engineering, 13(6), 120176. https://doi.org/10.1016/j.jece.2025.120176

Akhmadiyeva, N., Abikak, Y., Ramazanova, R., Orakbay, N., Abdulvaliyev, R., Burabayeva, N., Sagyntayeva, T., & Pozmogov, V. (2026). Joint thermochemical activation of nepheline ore and red mud: Phase transformations and alumina recovery. Minerals, 16(5), 434. https://doi.org/10.3390/min16050434

ASTM International. (2025). Standard practice for calculating yellowness and whiteness indices from instrumentally measured color coordinates (ASTM E313-20(2025)). https://doi.org/10.1520/E0313-20R25

Ayala, P., Borja, E. J., Magallón, L., Ramírez, J., & Sebastian, P. J. (2026). Hydrogen production by hydrolysis of recycled aluminum and reagent recovery by electrolysis of the by-product. Journal of Visualized Experiments, (230), e70270. https://doi.org/10.3791/70270

Bakhtom, A., Ghasemzade Bariki, S., Movahedirad, S., Charkhi, A., & Ghaffarinejad, A. (2023). Enhancement of the precipitation extent of $Al(OH)_3$ crystals in the Bayer process within a down-scaled tank. Hydrometallurgy, 222, 106166. https://doi.org/10.1016/j.hydromet.2023.106166

Bakhtom, A., Ghasemzade Bariki, S., Movahedirad, S., & Sobati, M. A. (2023). Machine learning-guided prediction and optimization of precipitation efficiency in the Bayer process. Chemical Papers, 77(5), 2509–2524. https://doi.org/10.1007/s11696-022-02642-x

Bakhtom, A., Ghasemzade Bariki, S., & Movahedirad, S. (2025). Exploring innovative strategies for precipitation extent enhancement in a downscaled Bayer process tank. The Canadian Journal of Chemical Engineering, 103(2), 941–952. https://doi.org/10.1002/cjce.25423

Bedar, A., Hlushko, H., Chen, P., Zhang, X., Wang, Z., Felsted, G., Feng, Y., Rosso, K. M., Pearce, C. I., & LaVerne, J. A. (2026). Radiation-induced surface modification of gibbsite in $NaNO_3$ environments. Journal of Physical Chemistry C, 130(32), 11201–11210. https://doi.org/10.1021/acs.jpcc.6c02488

Chen, B., Liu, G., Qi, T., Fu, Z., Shen, L., Wang, Y., Peng, Z., & Zhou, Q. (2024). Micelles and structural variation of the solution synergistically changing the viscosity of sodium aluminate solutions. Journal of Molecular Liquids, 400, 124557. https://doi.org/10.1016/j.molliq.2024.124557

JIRRS
Journal International Review of Research Studies

Received: 13/06/2026 - **Accepted:** 07/11/2026
Vol: 1.11
DOI: 10.66104/bwxmzv70
Pages: 1-36

Chen, F., Liu, F., Zhang, T., Liao, C., Wang, J., Zhang, J., & Wang, H. (2024). Selective separation and recovery of aluminum oxide from secondary aluminum dross by ammonium sulfate roasting transformation followed by cooling crystallization. Minerals Engineering, 216, 108866. https://doi.org/10.1016/j.mineng.2024.108866

Chen, P., Wang, S., Graham, T. R., Song, D., Zhao, X., Liu, L., Wang, Z., Pearce, C. I., Rosso, K. M., & Zhang, X. (2025). Unraveling anion-specific inhibition and structural modulation of gibbsite crystallization: Implications for aluminum mobility in natural and engineered systems. ACS Applied Materials & Interfaces, 17(46), 63987–63995. https://doi.org/10.1021/acsami.5c17528

Chen, P., Zhu, Y., Bergman, R., Xue, S., Zhao, Y., LaVerne, J., Guo, X., Pearce, C. I., Wang, Z., Chen, T., Rosso, K. M., & Zhang, X. (2024). Effects of ionizing radiation on the thermodynamic stability of boehmite and gibbsite. Journal of Physical Chemistry C, 128(8), 3578–3587. https://doi.org/10.1021/acs.jpcc.3c08456

Chen, S., Zhao, Z., Jiang, B., Zhang, Y., Wang, X., Xu, X., & Song, J. (2025). Synthesis of mesoporous alumina with high specific surface area via reverse precipitation method for enhanced adsorption and regeneration of Congo red. Materials, 18(11), 2656. https://doi.org/10.3390/ma18112656

Cheng, B., Sun, Y., Zhang, W., Wang, Y., Li, D., & Yang, R. (2025). Multi-layer core-shell ATH: A novel approach to flame retardant and high-performance EVA composites. Composites Communications, 53, 102224. https://doi.org/10.1016/j.coco.2024.102224

Dai, X., Qi, T., Li, X., Peng, Z., Liu, G., Zhou, Q., Wang, Y., & Shen, L. (2025). Efficient removal of fluorine in sodium aluminate solution via double salt crystallization process. Journal of Environmental Chemical Engineering, 13(1), 115269. https://doi.org/10.1016/j.jece.2024.115269

Damjanović, V., Stopić, S., Kostić, D., Perušić, M., Filipović, R., Mitrašinović, A., & Kostić, D. (2025). Removal of iron, zinc, and copper impurities from sodium aluminate after the Bayer process. Metals, 15(6), 669. https://doi.org/10.3390/met15060669

Diksha, D., & Khandelwal, N. (2026). Secondary mineral colloids genesis in mimicking post-COVID-19 surfactant-rich water bodies and impact on contaminant retention potential. Colloids and Surfaces A: Physicochemical and Engineering Aspects, 736, 139596. https://doi.org/10.1016/j.colsurfa.2026.139596

Doanh, T. C., Thi, N. H., Nguyen, H. T., Oanh, H. T., Doan, T. D., Tuyen, N. D., Vu, M., & Hoang, M. H. (2025). Preparation and synergistic effect of aluminum hydroxide nanoplates on the fire resistance and thermal stability of the intumescent flame retardant epoxy composite. RSC Advances, 15, 16814–16825. https://doi.org/10.1039/D5RA00231A

Dong, Y., Zhang, M., & Xie, C. (2020). Effect of reaction conditions on agglomeration of aluminum hydroxide in the recovery of waste aluminum catalyst. Separation and Purification Technology, 248, 116978. https://doi.org/10.1016/j.seppur.2020.116978

JIRRS
Journal International Review of Research Studies

Received: 13/06/2026 - **Accepted:** 07/11/2026
Vol: 1.11
DOI: 10.66104/bwxmzv70
Pages: 1-36

Dou, J., Xie, Y., Chen, R., & Qin, Y. (2025). Study on the dispersion and processing performance of activated aluminum hydroxide/ammonium polyphosphate composite flame retardant system for vinyl ester resin. Polymers, 17(5), 667. https://doi.org/10.3390/polym17050667

Dukarski, W., Krzyżanowski, P., Gonsior, M., & Rykowska, I. (2021). Flame retardancy properties and physicochemical characteristics of polyurea-based coatings containing flame retardants based on aluminum hydroxide, resorcinol bis(diphenyl phosphate), and tris (chloropropyl) phosphate. Materials, 14(18), 5168. https://doi.org/10.3390/ma14185168

Dyussenova, S., Gladyshev, S., Kuldeyev, E., Imangaliyeva, L., Fischer, D., Gemeal, A. M. B. M., Kasymzhanova, A., & Manapova, A. (2026). Processing of alumina production red mud sinter to produce solutions for carbonation. Processes, 14(15), 2504. https://doi.org/10.3390/pr14152504

Fadhilah, N., Wahyuono, R. A., Rois, M. F., & Risanti, D. D. (2025). Resolving two pathways of $Al(OH)_3$ formation in hydrogen production from aluminum-water reaction. International Journal of Hydrogen Energy, 143, 112–120. https://doi.org/10.1016/j.ijhydene.2025.05.311

Ferrante, F., Infurna, G., Battaglia, G., Tirelli, D., Campanelli, L., Micale, G., & Dintcheva, N. T. (2026). Toward advanced biocomposites based on thermoplastic biopolyester and halogen-free flame-retardant additives for industrial solutions. Macromolecular Materials and Engineering, 311(7), e70283. https://doi.org/10.1002/mame.70283

Fu, Z., Liu, G., Qi, T., Shen, L., Peng, Z., Li, X., Zhou, Q., & Wang, Y. (2024a). Cost-efficient removal of organics from Bayer liquor by tricalcium aluminate hexahydrate: Insights into the organic micelle and multilayer adsorption. Journal of Molecular Liquids, 125797. https://doi.org/10.1016/j.molliq.2024.125797

Fu, Z., Liu, G., Qi, T., Shen, L., Peng, Z., Li, X., Zhou, Q., & Wang, Y. (2024b). Efficient self-purification of anionic surfactants in Bayer liquor through a dense-ordered interfacial structure generated by trace amounts of cationic surfactants. Surfaces and Interfaces, 51, 104723. https://doi.org/10.1016/j.surfin.2024.104723

Fu, Z., Liu, G., Qi, T., Shen, L., Peng, Z., Zhou, Q., Wang, Y., Fang, H., & Wang, Y.-L. (2024). A short process for organic removal from sodium aluminate solution by regulating the electrical double layer of tricalcium aluminate hexahydrate. Transactions of Nonferrous Metals Society of China, 34(7), 2354–2366. https://doi.org/10.1016/S1003-6326(24)66546-5

Gao, H., Li, L., Huang, X., Kang, Z., Mao, M., Lin, Z., Chai, L., & Liu, W. (2026). Enhanced extraction of aluminum from secondary aluminum dross: Synergistic effects of two-step roasting with $(NH_4)_2SO_4$ and Na_2CO_3 on the activation of inert aluminum species. Surfaces and Interfaces, 91, 109305. https://doi.org/10.1016/j.surfin.2026.109305

Gao, Y., Li, M., Liu, Q., Liu, Z., Ma, W., Xie, K., Zhao, J., & Yan, H. (2026). Study on the behavior of potassium in bauxite during the digestion phase of the Bayer process. Minerals Engineering, 235(2), 109870. https://doi.org/10.1016/j.mineng.2025.109870

JIRRS
Journal International Review of Research Studies

Received: 13/06/2026 - **Accepted:** 07/11/2026
Vol: 1.11
DOI: 10.66104/bwxmzv70
Pages: 1-36

Gasparini, A. S., Fontes, M. P. F., Pacheco, A. A., & Ker, J. C. (2022). Gibbsite crystallinity and morphology in Ferralsols and bauxites. Minerals, 12(11), 1441. https://doi.org/10.3390/min12111441

Gladyshev, S., Dyussenova, S., Imangaliyeva, L., Fischer, D., Manapova, A., Kasymzhanova, A., & Bakirov, A. (2026). Production of aluminum hydroxide from aluminate solution obtained by red mud sinter processing via carbonation. Processes, 14(18), 2955. https://doi.org/10.3390/pr14182955

Golubev, V. O., & Litvinova, T. E. (2021). Dynamic simulation of industrial-scale gibbsite crystallization circuit. Journal of Mining Institute, 247, 88–101. https://doi.org/10.31897/PMI.2021.1.10

Gorla, G., Civati, F., Maurich, C., Brunello, V., Paganica, R., Rampazzi, L., & Giussani, B. (2022). New strategies to quantify aluminum hydroxide in powder coatings by thermogravimetric analysis and ATR-FT-MIR spectroscopy coupled with chemometrics. Microchemical Journal, 172, 107005. https://doi.org/10.1016/j.microc.2021.107005

Graham, T. R., Ghandi, K., Prange, M., Schenter, G., Anovitz, L. M., LaVerne, J. A., & Pearce, C. I. (2026). Detecting impurity-specific effects on structure and radiolytic hydrogen production in aluminum hydroxide. Chemical Communications, 62(2), 470–473. https://doi.org/10.1039/D5CC05272F

Graham, T. R., Hu, J. Z., Jaegers, N. R., Zhang, X., Pearce, C. I., & Rosso, K. M. (2022). An amorphous sodium aluminate hydrate phase mediates coordination change in highly alkaline sodium hydroxide solutions. Inorganic Chemistry Frontiers, 9(24), 6344–6357. https://doi.org/10.1039/D2QI01642G

Graham, T. R., Kennedy, A. R., Liu, W., Boglaienko, D. V., Felsted, R. G., Morton, J. G., Prange, M. P., Bowden, M. E., Lemmon, T. L., Swita, M. S., Wang, H.-W., Britton, M. D., Reynolds, J. G., Peterson, R. A., & Pearce, C. I. (2026). Gibbsite solubility and aluminum speciation in alkaline nuclear waste containing nitrate, nitrite, and phosphate. Chemical Engineering Journal, 177426. https://doi.org/10.1016/j.cej.2026.177426

Graham, T. R., Pouvreau, M., Gorniak, R., Wang, H.-W., Nienhuis, E. T., Miller, W., Liu, J., Prange, M. P., Schenter, G., Pearce, C. I., Rosso, K. M., & Clark, A. E. (2023). Disordered interfaces of alkaline aluminate salt hydrates provide glimpses of Al3+ coordination changes. Journal of Colloid and Interface Science, 637, 326–339. https://doi.org/10.1016/j.jcis.2023.01.003

Graham, T. R., Prange, M. P., Zhang, X., Bazak, J. D., Washton, N. M., Ghandi, K., Schenter, G. K., & Pearce, C. I. (2026). Localizing tetrahedral aluminum in nitrate-bearing gibbsite to constrain defect-impurity coupling. Inorganic Chemistry Frontiers, 13, 950–956. https://doi.org/10.1039/D5QI01703C

Guo, Q., Liu, Y., & Liu, S. (2026). Flame retardancy and smoke suppression of warm-mix asphalt binder containing various flame retardants. Coatings, 16(1), 15. https://doi.org/10.3390/coatings16010015

JIRRS
Journal International Review of Research Studies

Received: 13/06/2026 - **Accepted:** 07/11/2026
Vol: 1.11
DOI: 10.66104/bwxmzv70
Pages: 1-36

Guo, Q., Pouvreau, M., Rosso, K. M., & Clark, A. E. (2024). Mechanisms of dissolution from gibbsite step edges elucidated by ab initio molecular dynamics with enhanced sampling. Geochimica et Cosmochimica Acta, 366, 201–209. https://doi.org/10.1016/j.gca.2023.11.007

Guo, X., Chen, Y., Xue, S., Wang, Z., Li, J., Pan, X., Hua, M., & Jiang, J. (2025). Experimental research on the suppression of hydrogen deflagration by flame-retardant composite ultrafine dry powder fire extinguishing agents containing aluminum hydroxide. Process Safety and Environmental Protection, 198, 107121. https://doi.org/10.1016/j.psep.2025.107121

Guo, J., Xu, Y., Liu, H., Zhao, Q., Li, X., Zhang, M., & Yang, C. (2026). Radiation cross-linked polyurethane/aluminum hydroxide composites with high strength, self-healing, thermal insulation, and flame retardancy. Langmuir, 42(31), 22854–22867. https://doi.org/10.1021/acs.langmuir.6c02756

Gupta, R., Singh, M. K., Rangappa, S. M., Siengchin, S., Dhakal, H. N., & Zafar, S. (2024). Recent progress in additive inorganic flame retardants polymer composites: Degradation mechanisms, modeling and applications. Heliyon, 10(21), e39662. https://doi.org/10.1016/j.heliyon.2024.e39662

He, L., Bi, Q.-Q., Ma, Y., & Wang, D.-Y. (2025). Efficiently fire-safe asphalt achieved via synergistic effect of ferrocene and halloysite nanotube. Reactive and Functional Polymers, 210, 106197. https://doi.org/10.1016/j.reactfunctpolym.2025.106197

Hlushko, H., Ramos-Ballesteros, A., Bedar, A., Chen, P., Zhang, X., Colina Ruiz, R., Rosso, K. M., Pearce, C. I., & LaVerne, J. A. (2025). Radiolytic production of radical species in gibbsite doped with iron and chromium ions. Journal of Physical Chemistry C, 129(37), 16927–16937. https://doi.org/10.1021/acs.jpcc.5c05004

Hlushko, H., Ramos-Ballesteros, A., Chen, P., Zhang, X., Rosso, K. M., Pearce, C. I., & LaVerne, J. A. (2024). Effect of impurities on radical formation in gibbsite radiolysis. Physical Chemistry Chemical Physics, 26(13), 9867–9870. https://doi.org/10.1039/D3CP06305D

Hong, N., Chen, S., Liu, J., Li, F., Li, Y., Wang, L., & Ni, Y. (2026). Effects of surface-modified aluminum hydroxide on the mechanical properties, flame retardancy, and aging resistance of silicone rubber composites. High Performance Polymers, 38(1), 48–65. https://doi.org/10.1177/09540083251376561

Hu, F., Cheng, B., Cong, K., Li, D., Zhang, W., Qin, Z., & Yang, R. (2023). Enhancing char formation and flame retardancy of ethylene-vinyl acetate copolymer (EVA)/aluminum hydroxide (ATH) composites by grafting ladder phenyl/vinyl polysilsesquioxane (PhVPOSS). Polymers, 15(15), 3312. https://doi.org/10.3390/polym15153312

Huang, S., Chen, Y., Zhao, B., Wang, D., Gao, Q., Tian, Z., Chen, Z., & Luo, H. (2026). Stepwise recovery of aluminum and magnesium from secondary aluminum dross via alkali roasting and closed-loop ammonium sulfate leaching. Process Safety and Environmental Protection, 216, 109275. https://doi.org/10.1016/j.psep.2026.109275

JIRRS
Journal International Review of Research Studies

Received: 13/06/2026 - **Accepted:** 07/11/2026
Vol: 1.11
DOI: 10.66104/bwxmzv70
Pages: 1-36

Ilyas, R. A., Sapuan, S. M., Asyraf, M. R. M., Dayana, D. A. Z. N., Amelia, J. J. N., Rani, M. S. A., Norrrahim, M. N. F., Nurazzi, N. M., Aisyah, H. A., Sharma, S., Ishak, M. R., Rafidah, M., & Razman, M. R. (2021). Polymer composites filled with metal derivatives: A review of flame retardants. Polymers, 13(11), 1701. https://doi.org/10.3390/polym13111701

International Organization for Standardization & International Commission on Illumination. (2019). Colorimetry—Part 4: CIE 1976 $L^*_a*b^*$ colour space (ISO/CIE 11664-4:2019). https://www.iso.org/standard/74166.html

Ji, J., Ni, D., Shi, Y., Yang, Z., Ma, M., Zhu, S., & Wang, X. (2024). A simple method for preparing flame-retardant EVA/POE-g-MAH composites with high tensile strength by modified magnesium hydroxide and aluminum hydroxide. Journal of Applied Polymer Science, 141(24), e55505. https://doi.org/10.1002/app.55505

Jivkov, V., Petrova, B., Yavorov, N., & Makyov, Y. (2025). Flexural and specific properties of acrylic solid surface (PMMA/ATH) composites: Effects of thermoforming-relevant heating and cooling. Journal of Composites Science, 9(11), 620. https://doi.org/10.3390/jcs9110620

Kabir, I. I., Brehme, S., & Schartel, B. (2026). Multi-component coatings enabling low-toxicity and self-extinguishing polyurethane foams with potential for railway fire safety. Polymers, 18(17), 2096. https://doi.org/10.3390/polym18172096

Kim, S. J., Lee, J. I., Han, K. S., Byun, S. Y., Tran, T., & Kim, M. J. (2018). Recovery of fine aluminum hydroxide with high whiteness index from low quality bauxite using caustic roasting and water leaching. Korean Journal of Metals and Materials, 56(1), 49–58. https://doi.org/10.3365/KJMM.2018.56.1.49

Kuang, J., Liu, J., Pan, X., & Yu, H. (2026). Removal of impurity anions from sodium aluminate solution based on high-temperature desilication process. Hydrometallurgy, 241, 106648. https://doi.org/10.1016/j.hydromet.2026.106648

Li, M., Liu, Z., Yan, H., Ma, W., & Liu, S. (2024). Application of clean oxidation technology using H2O2 for simultaneous removal of sulfur and organic substances in the Bayer process. Hydrometallurgy, 106367. https://doi.org/10.1016/j.hydromet.2024.106367

Li, M., Liu, Z., Yan, H., Wei, J., & Liu, S. (2023). Removal of organic compounds from Bayer liquor by oxidation with sodium nitrate. Hydrometallurgy, 215, 105972. https://doi.org/10.1016/j.hydromet.2022.105972

Li, W., Li, J., Xing, H., Wang, K., Zhang, Y., & Liu, J. (2025). Simultaneously enhancing fire retardancy, acid and alkali resistance of polypropylene/aluminum trihydrate composite by microencapsulated red phosphorus. Journal of Vinyl and Additive Technology, 31(1), 199–210. https://doi.org/10.1002/vnl.22165

Li, X., Guo, Q., Zhao, Y., Qian, C., Pouvreau, M., Graham, T. R., Chen, P., Liu, L., Liu, C., Legg, B. A., Chen, Q., Miao, A., Wang, Z., De Yoreo, J. J., Pearce, C. I., Clark, A. E., Rosso, K. M., & Zhang, X. (2025). Mineral dissolution by dimeric complexes. Proceedings of the National Academy of Sciences, 122(41), e2504109122. https://doi.org/10.1073/pnas.2504109122

JIRRS
Journal International Review of Research Studies

Received: 13/06/2026 - **Accepted:** 07/11/2026
Vol: 1.11
DOI: 10.66104/bwxmzv70
Pages: 1-36

Li, X., Ho, T. A., Zhang, H., Liu, L., Li, R., Chen, P., Bowden, M. E., Mergelsberg, S. T., Fan, H., De Yoreo, J. J., Pearce, C. I., Rosso, K. M., & Zhang, X. (2025). Mesocrystal growth by oriented sliding and attachment of nanoplates. Nature Communications, 16, 11240. https://doi.org/10.1038/s41467-025-64852-7

Litvinova, T. E., & Tuleshov, N. V. (2026). Modeling of gibbsite solubility in Na+-K+-OH−-Al(OH)4−-SO42−-CO32− system applied to precipitation at sintering alumina refineries. Metals, 16(6), 633. https://doi.org/10.3390/met16060633

Litvinova, T. E., Golubev, V. O., & Tuleshov, N. V. (2026). PINN-PBE model for describing gibbsite crystallization dynamics. Metals, 16(8), 903. https://doi.org/10.3390/met16080903

Liu, J., Pan, X., Guo, Y., & Yu, H. (2025). Effect of impurity anions on selective separation of potassium from sodium aluminate solution via crystallization strategy. Materials Today Chemistry, 48, 103007. https://doi.org/10.1016/j.mtchem.2025.103007

Liu, J., Wang, Y., Pouvreau, M., Wang, J.-G., Liu, W., Chen, P., Zhou, Y., Wang, H.-W., Graham, T. R., Guo, X., Pearce, C. I., Wang, Z., Rosso, K. M., Zhu, Z., & Zhang, X. (2025). Direct observation of key aluminum hydroxide prenucleation oligomers for gibbsite nucleation and crystallization in sodium aluminate solution by liquid ToF-SIMS. Materials Today Chemistry, 44, 102596. https://doi.org/10.1016/j.mtchem.2025.102596

Liu, L., Chen, W., Fan, S., Xu, L., & Zhang, X. (2026). Enhanced removal of sodium oxalate from Bayer process spent liquor using fly ash: Insight into the adsorption mechanism. Separation and Purification Technology, 136862. https://doi.org/10.1016/j.seppur.2026.136862

Liu, L., Legg, B. A., Smith, W., Anovitz, L. M., Zhang, X., Harper, R., Pearce, C. I., Rosso, K. M., Stack, A. G., Bleuel, M., Mildner, D. F. R., Schenter, G. K., Clark, A. E., De Yoreo, J. J., Chun, J., & Nakouzi, E. (2023). Predicting outcomes of nanoparticle attachment by connecting atomistic, interfacial, particle, and aggregate scales. ACS Nano, 17(16), 15556–15567. https://doi.org/10.1021/acsnano.3c02145

Liu, R., Hou, H., Lin, Y., Yan, W., Hu, X., & Zi, F. (2025). Study on the efficient removal of trace iron from sodium aluminate solution by the heterogeneous nucleation method. Chemical Engineering Science, 316, 121993. https://doi.org/10.1016/j.ces.2025.121993

Liu, W., Pouvreau, M., Stack, A. G., Yang, X., & Clark, A. E. (2022). Concentration-dependent interfacial chemistry of the NaOH(aq): Gibbsite interface. Physical Chemistry Chemical Physics, 24(35), 20988–21008. https://doi.org/10.1039/D2CP01997C

Liu, Y., Tang, Z., & Zhu, J. (2022). Synergistic flame retardant effect of aluminum hydroxide and ammonium polyphosphate on epoxy resin. Journal of Applied Polymer Science, 139(46), e53168. https://doi.org/10.1002/app.53168

JIRRS
Journal International Review of Research Studies

Received: 13/06/2026 - **Accepted:** 07/11/2026
Vol: 1.11
DOI: 10.66104/bwxmzv70
Pages: 1-36

Liu, J., Pan, X., Chen, M., & Yu, H. (2024). A single-step crystallization process to remove potassium from sodium aluminate solution. Journal of Environmental Chemical Engineering, 12(5), 113330. https://doi.org/10.1016/j.jece.2024.113330

Liu, J., Pan, X., Wu, H., Hou, X., & Yu, H. (2024). Effect of inorganic anions on precipitation of desilication products based on low-temperature Bayer process. Transactions of Nonferrous Metals Society of China, 34(4), 1300–1310. https://doi.org/10.1016/S1003-6326(24)66472-1

Liu, S., Jiao, F., Liu, W., Li, C., Dong, L., Wang, H., & Qin, W. (2024). Experimental study on preparation of high-purity sodium aluminate with sodium aluminate solution. Mining and Metallurgical Engineering, 44(2), 100–105. https://doi.org/10.3969/j.issn.0253-6099.2024.02.025

Liu, J., Pan, X., & Yu, H. (2025). Crystallization and separation of potassium-containing salts in sodium aluminate solution. Proceedings of the 43rd International ICSOBA Conference (TRAVAUX 54), AA12. https://doi.org/10.71659/icsoba2025-aa012

Luo, N., Ju, J., Guo, W., Li, L., & An, J. (2025). Ultrasound-assisted hydrolysis of secondary aluminum dross and mechanism: Reducing environmental impact and improving resource recovery. Hydrometallurgy, 106627. https://doi.org/10.1016/j.hydromet.2025.106627

Ma, Y., Preveniou, A., Kladis, A., & Pettersen, J. B. (2022). Circular economy and life cycle assessment of alumina production: Simulation-based comparison of Pedersen and Bayer processes. Journal of Cleaner Production, 366, 132807. https://doi.org/10.1016/j.jclepro.2022.132807

Mahmud, A. A., Barua, T., Rafi, A. S., Rafi, A. M., Islam, M. A., Nuha, T. F., & Afif, A. (2026). Development of a lighter, durable, and fire-retardant composite material using epoxy, jute fiber, aluminum hydroxide, recycled PET plastics, and rice husk ash. Next Research. https://doi.org/10.1016/j.nexres.2026.101502

Malucelli, G. (2025). Flame retardant surface treatments for rigid polyurethane foams used in the building sector: Current state-of-the-art and perspectives. Construction and Building Materials, 140947. https://doi.org/10.1016/j.conbuildmat.2025.140947

Marinos, D., Kotsanis, D., Alexandri, A., Balomenos, E., & Panias, D. (2021). Carbonation of sodium aluminate/sodium carbonate solutions for precipitation of alumina hydrates—Avoiding dawsonite formation. Crystals, 11(7), 836. https://doi.org/10.3390/cryst11070836

Marinos, D., Kotsanis, D., van der Eijk, C., Balomenos, E., & Panias, D. (2025). Alumina recovery from sodium aluminate solutions via carbonation. Proceedings of the 43rd International ICSOBA Conference (TRAVAUX 54), AA09. https://doi.org/10.71659/icsoba2025-aa009

Meng, L., & Zhang, L. (2025). Hydrogen bonding adsorption principle in caustic solution of aluminum hydroxide. Proceedings of the 43rd International ICSOBA Conference (TRAVAUX 54), AA07. https://doi.org/10.71659/icsoba2025-aa007

JIRRS
Journal International Review of Research Studies

Received: 13/06/2026 - **Accepted:** 07/11/2026
Vol: 1.11
DOI: 10.66104/bwxmzv70
Pages: 1-36

Moreno, R. A. (2020). Purificação do licor Bayer: Remoção de impurezas orgânicas e inorgânicas para aumentar a produtividade e tratar os resíduos gerados neste processo. Dissertação de mestrado, Universidade de São Paulo. https://doi.org/10.11606/D.3.2020.tde-22012021-130010

Mwase, J. M., Vafeias, M., Marinos, D., Dimitrios, P., & Safarian, J. (2022). Investigating aluminum tri-hydroxide production from sodium aluminate solutions in the Pedersen process. Processes, 10(7), 1370. https://doi.org/10.3390/pr10071370

Nalivaiko, A. Y., Ozherelkov, D., Pak, V. I., & Kirov, S. S. (2020). Preparation of aluminum hydroxide during the synthesis of high-purity alumina via aluminum anodic oxidation. Metallurgical and Materials Transactions B, 51(3), 1154–1161. https://doi.org/10.1007/s11663-020-01829-5

Nasirzadeh, M., Ebrahimi, M., & Zahedi, S. (2025). Enhancing the durability of fire-retardant epoxy coatings through an eco-friendly self-stratification approach. Journal of Coatings Technology and Research, 22, 1699–1712. https://doi.org/10.1007/s11998-025-01073-z

Nienhuis, E. T., Pouvreau, M., Graham, T. R., Prange, M. P., Page, K., Loring, J. S., Stack, A. G., Clark, A. E., Schenter, G. K., Rosso, K. M., Pearce, C. I., & Wang, H.-W. (2022). Structure and reactivity of sodium aluminate complexes in alkaline solutions. Journal of Molecular Liquids, 367, 120379. https://doi.org/10.1016/j.molliq.2022.120379

Pereira, A. C. (2026a). Bauxite Residue (Red Mud) from the Bayer Process: A Critical Review of Management, Safe Storage, Valorization, Critical-Metal Recovery, and Industrial Integration. Journal International Review of Research Studies, 1(10 - October), 1–46. https://doi.org/10.66104/90twks68

Pereira, A. C. (2026b). Controlling co-precipitation in hydrometallurgy: From physicochemical parameters to process design and technology readiness. IKR Journal of Engineering and Technology, 2, 46–77. https://doi.org/10.5281/zenodo.20357561

Pereira, A. C. (2026c). Improving filterability of hydroxide precipitates in hydrometallurgical hydrolysis processes: A critical review. IKR Journal of Engineering and Technology, 2, 21–45. https://doi.org/10.5281/zenodo.20098962

Pereira, A. C. (2026d). Scale-up in mineral processing: From mechanism preservation to flowsheet-scale transferability—A critical review and the MINESCALE framework. Journal of Advanced Multidisciplinary Studies (JAMS), 1(III), 661–694. https://jamsjournal.org/JAMS/article/view/800

Pereira, A. C. (2026e). Secondary aluminum dross and salt slag treatment: A critical review of integrated value recovery, risk control, and industrial readiness. International Journal of Current Science Research and Review, 9(8), 4428–4462. https://doi.org/10.5281/zenodo.21898845

JIRRS
Journal International Review of Research Studies

Received: 13/06/2026 - **Accepted:** 07/11/2026
Vol: 1.11
DOI: 10.66104/bwxmzv70
Pages: 1-36

Pouvreau, M., Guo, Q., Wang, H.-W., Schenter, G. K., Pearce, C. I., Clark, A. E., & Rosso, K. M. (2023). An efficient reactive force field without explicit coordination dependence for studying caustic aluminum chemistry. Journal of Physical Chemistry Letters, 14, 6743–6748. https://doi.org/10.1021/acs.jpclett.3c01176

Rai, S., Pradhan, P., Panchal, M., Mankar, A., & Agnihotri, A. (2025). An alternative approach for production of non-metallurgical grade aluminum hydroxide utilizing low-grade bauxite. Proceedings of the 43rd International ICSOBA Conference (TRAVAUX 54), AA15. https://doi.org/10.71659/icsoba2025-aa015

Ran, J., Duan, H., Srinivasakannan, C., Yao, J., Yin, S., & Zhang, L. (2022). Effective removal of organics from Bayer liquor through combined sonolysis and ozonation: Kinetics and mechanism. Ultrasonics Sonochemistry, 88, 106106. https://doi.org/10.1016/j.ultsonch.2022.106106

Ran, J., Duan, H., Yao, J., Li, Y., & Yin, S. (2022). Recent progress in the removal of organic matter from Bayer liquor by advanced oxidation processes. Journal of Beijing University of Chemical Technology (Natural Science), 49(2), 1–12. https://doi.org/10.13543/j.bhxbzr.2022.02.001

Scionti, G., Piperopoulos, E., Atria, M., Calabrese, L., & Proverbio, E. (2023). Effect of magnesium hydroxide and aluminum hydroxide as thermal barriers on the flame-retardant behavior of acrylic-based coating. Coatings, 13(9), 1517. https://doi.org/10.3390/coatings13091517

Setyanto, D., Jayatun, Y. A., Basoeki, P. D., & De Fretes, A. (2022). Physical properties of glass-fiber-reinforced polymer filled with alumina trihydrate and calcium carbonate. Polymers, 14(12), 2464. https://doi.org/10.3390/polym14122464

Shaker, K., Adnan, M., Nawab, Y., Umair, M., Jabbar, M., Siddique, A., & Ahmad, A. (2023). Mechanical performance of glass/epoxy composites loaded with silane-treated aluminum hydroxide fillers. Polymers, 15(17), 3514. https://doi.org/10.3390/polym15173514

Shoppert, A., Valeev, D., Alekseev, K., & Loginova, I. (2023). Enhanced precipitation of gibbsite from sodium aluminate solution by adding agglomerated active $Al(OH)_3$ seed. Metals, 13(2), 193. https://doi.org/10.3390/met13020193

Silva, F. K., Boca Santa, R. A. A., Fiori, M. A., de Aquino, T. F., Soares, C., Martins, M. A. P. M., Padoin, N., & Riella, H. G. (2020). Synthesis of aluminum hydroxide nanoparticles from the residue of aluminum anodization for application in polymer materials as antiflame agents. Journal of Materials Research and Technology, 9(4), 8937–8952. https://doi.org/10.1016/j.jmrt.2020.05.108

Sonthalia, R., Behara, P., Kumaresan, T., & Thakre, S. (2013). Review on alumina trihydrate precipitation mechanisms and effect of Bayer impurities on hydrate particle growth rate. International Journal of Mineral Processing, 125, 137–148. https://doi.org/10.1016/j.minpro.2013.08.002

JIRRS
Journal International Review of Research Studies

Received: 13/06/2026 - **Accepted:** 07/11/2026
Vol: 1.11
DOI: 10.66104/bwxmzv70
Pages: 1-36

Soplin Pastor, M. A. (2021). Utilização da ozonização como processo de oxidação avançada para a remoção da matéria orgânica do licor Bayer. Dissertação de mestrado, Universidade de São Paulo. https://doi.org/10.11606/D.3.2021.tde-08042021-102203

Sung, K.-S., & Kim, N. (2023). Synergistic improvement of flame retardancy and mechanical properties of epoxy/benzoxazine/aluminum trihydrate adhesive composites. Polymers, 15(11), 2452. https://doi.org/10.3390/polym15112452

Sung, K.-S., Cho, H.-W., Kwon, K.-H., & Kim, N. (2026). Tailoring flame retardance and thermal conductivity of epoxy/benzoxazine mixtures via aluminum trihydrate and ceramic hybridization. Polymers, 18(5), 648. https://doi.org/10.3390/polym18050648

Sung, K.-S., Cho, H.-W., Lee, D.-H., Kim, W., & Kim, N. (2024). Fire-resistant and thermal stability properties of fluorosilicone adhesives by incorporation of surface-modified aluminum trihydrate. Polymers, 16(17), 2510. https://doi.org/10.3390/polym16172510

Tang, J., Liu, G., Qi, T., Zhou, Q., Peng, Z., Li, X., Yan, H., & Hao, H. (2022). Two-stage process for the safe utilization of secondary aluminum dross in combination with the Bayer process. Hydrometallurgy, 209, 105836. https://doi.org/10.1016/j.hydromet.2022.105836

Tang, Y., Ma, L., Qiu, Z., Yang, W., Chen, B., & Lin, Y. (2024). Research on synergistic disposal and high-value utilization of secondary aluminum dross and spent carbon anode. Process Safety and Environmental Protection, 184, 1094–1105. https://doi.org/10.1016/j.psep.2024.02.040

Uddin, M., Alabbad, M., Li, L., Orell, O., Sarlin, E., & Haapala, A. (2022). Novel micronized mica-modified casein–aluminum hydroxide as fire-retardant coatings for wood products. Coatings, 12(5), 673. https://doi.org/10.3390/coatings12050673

Wang, H.-W., Nienhuis, E. T., Graham, T. R., Pouvreau, M., Reynolds, J. G., Bowden, M. E., Schenter, G. K., De Yoreo, J. J., Rosso, K. M., & Pearce, C. I. (2024). Resolving intermediates during the growth of aluminum deuteroxide (hydroxide) polymorphs in high chemical potential solutions. Communications Chemistry, 7, 199. https://doi.org/10.1038/s42004-024-01285-1

Wang, H.-W., Prange, M. P., Graham, T. R., Zhang, X., Daemen, L., Kolesnikov, A. I., Schenter, G. K., Anovitz, L. M., Rosso, K. M., & Pearce, C. I. (2025). Liberation of hydroxyl groups in layered aluminum (oxy)hydroxides and other material analogs: Insights from inelastic neutron scattering and theory. Physical Chemistry Chemical Physics. https://doi.org/10.1039/D5CP03788C

Wang, Q., Huang, J., & Chang, Q. (2025). Flame retardancy and smoke suppression of rigid polyurethane foam based on a synergistic expansion composite system with modified aluminum hydroxide. ChemistrySelect, 10, e202500003. https://doi.org/10.1002/slct.202500003

Wang, R., Zhang, Y., Wang, N., & Wu, Y. (2024). Rate-dependent tensile properties of aluminum-hydroxide-enhanced ethylene propylene diene monomer coatings for solid rocket motors. Materials, 17(15), 3790. https://doi.org/10.3390/ma17153790

JIRRS
Journal International Review of Research Studies

Received: 13/06/2026 - **Accepted:** 07/11/2026
Vol: 1.11
DOI: 10.66104/bwxmzv70
Pages: 1-36

Wen, J., Liu, G., Qi, T., Liu, N., Zhou, Q., Guo, J., Shen, L., & Wang, Y. (2026). Sodium elimination from Bayer gibbsite to prepare high-purity alumina through aluminum coordination and pore structure regulation. Materials Today Chemistry, 52, 103447. https://doi.org/10.1016/j.mtchem.2026.103447

Wen, J., Liu, G., Qi, T., Zhou, Q., Peng, Z., Li, X., Wang, Y., & Shen, L. (2026). Precipitation of the ultrafine equiaxial near-spherical gibbsite with low oil absorption value by adding mixed seeds. Hydrometallurgy, Article 106586. https://doi.org/10.1016/j.hydromet.2025.106586

Wen, J., Liu, G., Qi, T., Liu, N., Zhou, Q., Guo, J., Shen, L., & Wang, Y. (2025). Design and reinforcement mechanisms of the binary alumina ceramics with improved density derived from industrial gibbsite and boehmite. Journal of Alloys and Compounds, 184571. https://doi.org/10.1016/j.jallcom.2025.184571

Wu, P., Liu, G., Li, X., Peng, Z., Zhou, Q., Qi, T., Wang, Y., & Shen, L. (2022). Removal of organics from Bayer liquors via foam flotation. Journal of Cleaner Production, 130353. https://doi.org/10.1016/j.jclepro.2021.130353

Wu, Q., Wu, L., Li, H., & Dong, Y. (2025). Disposal of reactive compounds and salts in secondary aluminum dross: A critical review. Process Safety and Environmental Protection, 198, 107158. https://doi.org/10.1016/j.psep.2025.107158

Wu, X., Zhen, A., Zhang, Q., Li, X., Zhou, Q., Qi, T., & Liao, K. (2024). Kinetics of active seed-induced $Al(OH)_3$ precipitation from $NaAlO_2$ solution for recycling aluminum from spent lithium-ion batteries. Energy & Fuels, 38(15), 14704–14711. https://doi.org/10.1021/acs.energyfuels.4c02346

Xie, J., Qin, Q., Sheng, A., Shi, H., Yin, H., Zheng, K., Xie, L., Liu, W., & Li, Y. (2026). Adsorption of gallium from bauxite Bayer liquor using acrylonitrile–divinylbenzene–amidoxime resin and deactivation after multiple cycles due to an aluminum hydroxide layer. Hydrometallurgy, 106748. https://doi.org/10.1016/j.hydromet.2026.106748

Xing, H., Li, J., Liu, M., Qi, J., Liu, J., Luo, J., & Cui, F. (2025). Flame retardancy and mechanical properties of ethylene vinyl acetate copolymer containing aluminum trihydrate: The impact of the polymer matrix. Materials Today Communications, 44, 112153. https://doi.org/10.1016/j.mtcomm.2025.112153

Xing, H., Li, J., Liu, M., Yang, X., Liu, J., Pan, B., & Chang, H. (2025). Simultaneously enhanced flame retardancy, mechanical properties, and acid/alkali corrosion resistance of ethylene vinyl acetate/aluminum trihydrate composite induced by crosslinking and microencapsulated expandable graphite. Polymer Degradation and Stability, 234, 111263. https://doi.org/10.1016/j.polymdegradstab.2025.111263

Xing, H., Yu, Z., Liu, M., Yang, X., Liu, J., Chang, H., & Pan, B. (2025). A novel strategy to endow aluminum trihydrate-filled ethylene vinyl acetate composite with excellent flame retardancy, mechanical properties, and acid/alkali corrosion resistance concurrently. Composites Communications, 55, 102329. https://doi.org/10.1016/j.coco.2025.102329

JIRRS
Journal International Review of Research Studies

Received: 13/06/2026 - **Accepted:** 07/11/2026
Vol: 1.11
DOI: 10.66104/bwxmzv70
Pages: 1-36

Xu, L., Chen, W.-M., Zhang, Y.-J., Fan, S., Pi, J.-Q., & Wang, M.-L. (2024). Effect of zinc(II) and caustic content on the decomposition of sodium aluminate solutions and relevance to the Bayer process. Hydrometallurgy, 225, 106287. https://doi.org/10.1016/j.hydromet.2024.106287

Xu, Y., Bao, W., Ding, H., & Qu, J. (2023). Preparation of $CaCO_3$/$Al(OH)_3$ composites via heterogeneous nucleation. Materials, 16(2), 498. https://doi.org/10.3390/ma16020498

Yang, M., & Yuan, B. (2025). Modification of aluminum hydroxide by ball milling: A feasible method to obtain high-efficiency flame retardants for production of high-performance EVA composites. Materials, 18(5), 984. https://doi.org/10.3390/ma18050984

Yang, X., Du, G., Shuai, H., Xu, X., & Wang, J. (2025). Study on the mechanical and thermal properties of waterborne polyurethane-modified aluminum hydroxide and its application in LDPE plastics. Polymers, 17(5), 556. https://doi.org/10.3390/polym17050556

Yang, Z., Zhou, Q., Peng, Z., Liu, G., Qi, T., Li, X., Shen, L., & Wang, Y. (2024). Bayerite in aluminum hydroxide affects the thermal decomposition pathways and reduces the density of α-Al2O3. Journal of Alloys and Compounds, 1004, 175884. https://doi.org/10.1016/j.jallcom.2024.175884

Yao, H., Wang, N., Chen, M., & Chen, X. (2026). Hydrothermal synthesis of hierarchical boehmite from co-processed stainless steel dust and aluminum dross residue. Metals, 16(5), 455. https://doi.org/10.3390/met16050455

Yin, F., Ma, K., Gan, X., Li, L., Zhang, H., & Lu, L. (2026). Investigation of the mechanical performance and flame retardancy of polymer cement-based coatings with ettringite modified by an amphiphilic group. Polymers, 18(7), 863. https://doi.org/10.3390/polym18070863

Yuan, B., Jin, H., Kong, Y., Xu, X., & Yang, M. (2024). Gelatin-based ionic hydrogel for intelligent fire-alarm system with considerable toughness, flame retardancy, and thermoelectric performance. International Journal of Biological Macromolecules, 278, 135006. https://doi.org/10.1016/j.ijbiomac.2024.135006

Yuksel Yilmaz, A. N., Akgul, S., & Celik Bedeloglu, A. (2026). Effects of zinc borate, aluminum hydroxide, and magnesium hydroxide on the flame-retardant performance and mechanical properties of glass fiber-reinforced epoxy composites. Fire and Materials, 1–12. https://doi.org/10.1002/fam.70098

Zachara, T., Borůvka, V., Kytka, T., Petržela, B., Kubista, K., & Šedivka, P. (2026). Fire safety assessment of insulation boards made from recycled cotton fibers: Part I—Thermal properties and fire behavior. Fire, 9(9), 394. https://doi.org/10.3390/fire9090394

Zain, N. M., Ghazali, F. A., Che Lah, N. A., & Hussin, M. H. (2025). Effect of aluminum hydroxide on the physical, mechanical, and fire-resistant properties of Acacia mangium waste/polyurethane particleboards. International Journal of Adhesion and Adhesives, 143, 104174. https://doi.org/10.1016/j.ijadhadh.2025.104174

JIRRS
Journal International Review of Research Studies

Received: 13/06/2026 - **Accepted:** 07/11/2026
Vol: 1.11
DOI: 10.66104/bwxmzv70
Pages: 1-36

Zainudin, M., Diharjo, K., Kaavessina, M., Setyanto, D., & Ubaidillah, U. (2022). Industrial implementation of aluminum trihydrate-fiber composition for fire resistance and mechanical properties in glass-fiber-reinforced polymer roofs. Polymers, 14(7), 1273. https://doi.org/10.3390/polym14071273

Zhang, C., Liu, Y., Guo, S., Li, Y., Wang, S., Cheng, S., & Shen, H. (2025). Utilization of CO2 as a precipitant to prepare aluminum hydroxide from NaAl(OH)4 solutions: Study on reaction kinetics and mechanism. Hydrometallurgy, 234, 106473. https://doi.org/10.1016/j.hydromet.2025.106473

Zhang, H., Wang, Z., Zhao, Y., Cui, W., Zhang, X., Wang, S., Walter, E. D., Sassi, M. J., Pearce, C. I., Clark, S. B., & Rosso, K. M. (2023). Metal ion (Cr3+, Eu3+, UO2 2+) adsorption on gibbsite nanoplates. Engineered Science, 24, 896. https://doi.org/10.30919/es896

Zhang, J., Xu, S., Han, X., Chai, R., Zhang, F., Tian, S., Fan, H., & Du, S. (2024). Preparation of near-spherical α-Al2O3 particles by enhanced precipitation of gibbsite from sodium aluminate solution using highly dispersed Al2O3 as seeds. Inorganic Chemistry, 63(42), 19744–19751. https://doi.org/10.1021/acs.inorgchem.4c02970

Zhang, S., Sheng, Y., Lin, X., Ma, L., Wang, Z., Wang, Q., & Hu, D. (2024). Rheological properties of fluorine-free foams stabilized by aluminum hydroxide nanoparticles and a mixture of siloxane and hydrocarbon surfactants. Journal of Molecular Liquids, 401, 124627. https://doi.org/10.1016/j.molliq.2024.124627

Zhang, Y., Lin, K., Su, Z., Xu, J., & Jiang, T. (2023). Self-driven hydrolysis mechanism of secondary aluminum dross (SAD) in the hydrometallurgical process without any additives. Chemical Engineering Journal, 466, 143141. https://doi.org/10.1016/j.cej.2023.143141

Zhang, Y., Xu, R., Tang, H., Wang, L., & Sun, W. (2020). A review on approaches for hazardous organics removal from Bayer liquors. Journal of Hazardous Materials, 397, 122772. https://doi.org/10.1016/j.jhazmat.2020.122772

Zhao, X., Guillen, T. R., Graham, T. R., Chen, P., Zhao, Y., Mergelsberg, S. T., Zhu, Z., Wang, Z., Rosso, K. M., Guo, X., & Zhang, X. (2024). Incorporation of rare earth elements Sc, Y, and La into gibbsite. Chemical Engineering Journal, 485, 149809. https://doi.org/10.1016/j.cej.2024.149809

Zhao, Y., Prange, M. P., Zong, M., Wang, Y., Walter, E., Chen, Y., Zhu, Z., Engelhard, M. H., Wang, X., Zhao, X., Pearce, C. I., Miao, A., Wang, Z., Rosso, K. M., & Zhang, X. (2024). Understanding trace iron and chromium incorporation during gibbsite crystallization and effects on mineral dissolution. Environmental Science & Technology, 58(45), 20125–20136. https://doi.org/10.1021/acs.est.4c04483

Zheng, P., Yang, Z., Zhao, H., Bian, A., Zhou, Y., He, J., & Liu, Q. (2025). Silica-based Schiff base-modified aluminum hydroxide for excellent flame retardancy and char formation in thermoplastic polyolefins. Polymer, 336, 128917. https://doi.org/10.1016/j.polymer.2025.128917

JIRRS
Journal International Review of Research Studies

Received: 13/06/2026 - **Accepted:** 07/11/2026
Vol: 1.11
DOI: 10.66104/bwxmzv70
Pages: 1-36

Zheng, S., Lu, Y., & Zhao, H. (2025). Green synthesis and particle size control of high-purity alumina based on hydrolysis of alkyl aluminum. Materials, 18(9), 2100. https://doi.org/10.3390/ma18092100

Zheng, X., Yuan, F., Ma, A., & Tian, S. (2024). Experimental study on microwave drying aluminum hydroxide. Coatings, 14(6), 687. https://doi.org/10.3390/coatings14060687

Zheng, Y., Gu, F., Wang, Z., Zhou, Y., Xu, L., & Hall, P. (2025). A comparative study on the mechanical and flammability properties of aluminum hydroxide and hollow glass bead-filled polypropylene composites. Journal of Vinyl and Additive Technology, 31(1), 182–198. https://doi.org/10.1002/vnl.22164

Zhou, G.-T., Wang, Y.-L., Qi, T.-G., Zhou, Q.-S., Liu, G.-H., Peng, Z.-H., & Li, X.-B. (2023). Toward sustainable green alumina production: A critical review on process discharge reduction from gibbsitic bauxite and large-scale applications of red mud. Journal of Environmental Chemical Engineering, 11(2), 109433. https://doi.org/10.1016/j.jece.2023.109433

Zhu, K., Yang, Y., Lin, C., Wang, Q., Ye, D., Jiang, H., & Wu, K. (2024). Effect of compounded aluminum hydroxide flame retardants on the flammability and smoke suppression performance of asphalt binders. ACS Omega, 9(2), 2803–2814. https://doi.org/10.1021/acsomega.3c08094

Zielonka, P., Duda, S., Lesiuk, G., Błażejewski, W., Wiśniewska, M., Warycha, J., Stabla, P., Smolnicki, M., & Babiarczuk, B. (2022). The effect of flame retardant—Aluminum trihydroxide on mixed mode I/II fracture toughness of epoxy resin. Polymers, 14(20), 4386. https://doi.org/10.3390/polym14204386